References

AL HADDAD, M. & BECKER, P. J. (1988). *Acta Cryst.* A**44**, 262–270.
AL HADDAD, M. & BECKER, P. (1990). *Acta Cryst.* A**46**, 112–123.
BECKER, P. (1977). *Acta Cryst.* A**33**, 667–671.
BECKER, P. & AL HADDAD, M. (1989). *Acta Cryst.* A**45**, 333–337.
BECKER, P. & AL HADDAD, M. (1990). *Acta Cryst.* A**46**, 123–129.
GUIGAY, J. P. (1989). *Acta Cryst.* A**45**, 241–244.
KATO, N. (1976). *Acta Cryst.* A**32**, 453–466.
KATO, N. (1980). *Acta Cryst.* A**36**, 763–769, 770–778.
MESSOLORAS, S., SCHNEIDER, R. J., STEWART, R. J. & ZULEHNER, W. (1988). *Nature (London)*, **336**, 376–365.
SCHNEIDER, J. R., CONÇALVES, O. D. & GRAF, H. A. (1988). *Acta Cryst.* A**44**, 461–467.
SCHNEIDER, J. R., CONÇALVES, O. D., ROLLASON, A. J., BONSE, U., LAUER, J. & ZULEHNER, W. (1988). *Nucl. Instrum. Methods Phys. Res.* B**29**, 661–674.

Acta Cryst. (1992). A**48**, 134–158

Modern Equations of Diffractometry. Diffraction Geometry*

BY D. J. THOMAS†

Medical Research Council Laboratory of Molecular Biology, Hills Road, Cambridge CB2 2QH, England

(*Received* 26 *June* 1990; *accepted* 29 *July* 1991)

Abstract

The various geometries of area-detector diffractometers and cameras are best described using a coordinate-free abstract operator notation. Modern methods of geometry, including especially the combined application of vectors and covectors, are used; they confer the simultaneous advantages of simplifying, virtualizing and unifying the analysis, which becomes applicable to all methods and machines. A second, and most valuable, prize arising from this approach, itself a major theme of this paper, is the complete avoidance of computationally expensive and analytically inconvenient trigonometric functions in area diffractometry. The very few occasions when they are unavoidable have already been discussed fully in a previous paper on goniometry. Basic diffraction geometry is presented first, giving all the equations necessary to identify diffraction spots and to calculate a useful generalization of the Lorentz factor. These are a formalized and extended version of those presented to the EEC Cooperative Workshop on Position-Sensitive Detector Software held at LURE in Paris in 1986. Then, various previously unpublished formulae describing beam divergence, dispersion and polarization, crystal mosaicity and angular widths of diffraction spots are presented. Finally, three specific calculations appropriate to the use of an area diffractometer are given, including a calculation of window sizes, a model of the backstop shadow and a method of surveying a diffraction pattern for assessment and prealignment.

1. Introduction – unification through generalization

From the earliest days of crystallographic diffraction studies, the analysis of diffraction geometry has been heavily reliant on the use of trigonometric functions and of radical forms, particularly the square root. This was because, at a time when electronic computers were not available, roots and trigonometric functions could conveniently be read from tables, whereas equivalent vectorial (*i.e.* matrix) calculations would have been intolerably tedious. With the advent of digital computers, particularly in demanding 'real-time' applications, radical and trigonometric calculations became relatively less favourable when compared with component calculations using vectors and matrices, which are the natural variables for 'area detectors'.‡ Although cameras existed and were in common use, they were not perceived as area detectors until their electronic successors appeared. Thus, it did not become apparent until fairly recently that any theory of area diffractometry based on vectorial calculations could exist in contradistinction to that of single-counter diffractometry, where the use of angular variables is entirely natural.

It was not until 1986 at the EEC Cooperative Workshop on Position-Sensitive Detectors in Paris that it became apparent that the simple vectorial equations long used in the Cambridge software package for the Enraf–Nonius FAST system were not, in fact, common knowledge. I was thus encouraged to make them more widely known, and hope that this paper achieves that. At the same workshop, Dr Gérard Bricogne used the term 'virtualized'

* This paper is a sequel to Modern Equations of Diffractometry. Goniometry [*Acta Cryst.* (1990), A**46**, 321–343] in which it is referred to as Thomas (1990*b*). The second author with M. R. Hestenes in the reference list to that paper (p. 342) should have been E. Stiefel.

† Present address: European Molecular Biology Laboratory, Meyerhofstrasse 1, Postfach 10.2209, W-6900 Heidelberg, Germany.

‡ The misnomer 'area detector' (*cf.* 'linear detector', 'single counter') is the accepted name for a 2D imaging detector for recording diffraction patterns. It usually also bears the connotation of a reusable electronically readable device, which in some way justifies the need for a special name; in the present paper the term has a more general meaning and is held to include any detector capable of measuring a 2D image, including film.

0108-7673/92/020134-25$03.00

to describe the way that this simple vectorial approach unified the analysis of all machines, enabling the use of a common set of equations. In the intervening five years, the geometrical structure of the equations has become clearer and the notational representation has been formalized further.

The importance of a concise and lucid notation is a major theme of the development, and the much less fundamental component representations are given only to help in numerical computations. The novel symmetry-based metric-invariant notation for rotational calculations expounded in a previous paper on goniometry [Thomas, 1990*a* (referred to hereafter as *Goniometry*)] is used to achieve that purpose. To summarize, it is based on characteristically shaped symbolic operators performing functions as follows: projection onto a line using $\cdot|\cdot$; projection onto a plane using $\cdot\lfloor\cdot$; projection onto a plane with attendant right-rotation using $\cdot\int\cdot$ or its inverse $\cdot\rceil\cdot$; and finally projection onto a plane with a rotation through half a turn using $\cdot\top\cdot$. This is shown diagramatically in Fig. 1 which is derived from Fig.3 of the previous paper. In use, the missing argument symbol $\cdot$ is replaced by the algebraic name of the intended line or axis. The double occurrence of the name conveys the metric invariance of the operators; if one occurrence be held to induce a dependence upon a metric, then the other is held to cancel it by being mutually contravariant; in other words, if one symbol multiplies, the other divides. Thus all of these operators are idempotent. Table 1 gives a list of general symbols.

The discussion here is aimed at a greater geometrical rigour than has been usual hitherto, which demands the extensive use of covectors in addition to the more familiar use of vectors proper. The concept of a covector is an important one: a covector is defined to be such that it can act on a vector to produce a scalar, which means that it is naturally susceptible to representation by series of contour planes (see Burke, 1985, pp. 18–21, 27–31). This is in strict contradistinction to the well established but geometrically nonsensical convention where two vectors can apparently act upon each other to produce a scalar using the dot product notation. These concepts are described succinctly in much greater detail than can be done here in the first few pages of the book by Burke just cited.

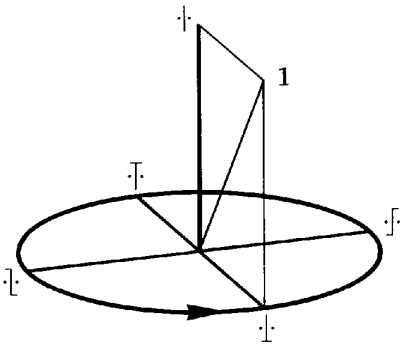

Fig. 1. An indicator diagram for the rotational operators. This shows geometrically the invariant operator $\cdot|\cdot$ which projects its vector argument onto a line such as an axis of rotation and the skew operators $\cdot\int\cdot$ and $\cdot\lfloor\cdot$ which project their vector arguments onto a plane such as an orbital plane as shown here with an attendant right-rotation. The symmetric operator $\cdot\lfloor\cdot$ similarly projects onto the same plane, but with no attendant rotation, whilst the antisymmetric operator $\cdot\top\cdot$ projects with a rotation of half a turn. The identity operator, **1**, marks the unaltered operand in its original position.

The more modern understanding is that the dot product works only by virtue of a hidden but implicit metric tensor, say $\mathcal{G}$, so that the familiar $\mathbf{a}\cdot\mathbf{b}$ is more properly $\mathbf{a}\mathcal{G}\mathbf{b} \equiv (\mathcal{G}\mathbf{a})\mathbf{b}$, fortunately having $\mathcal{G} = \mathbf{1}$ (the multiplicative identity) so long as the space involved is Cartesian–Euclidean and properly scaled and dimensioned. These geometries are shown in Figs. 2 and 3. Even when numerically 1, the metric tensor is intrinsically a dimensioned quantity, which is a good reason for using it.

The singular advantage of the more modern metric invariant vector–covector formalism derived from the field of applied differential geometry is that considerations of the metric tensor become irrelevant. Covectors and vectors are geometrical duals of each other and their computational representations are related by the generalized inverse. Seen this way, it becomes obvious that a vector being acted upon by a covector which happens to be its own inverse simply yields the dimensionless metric-invariant unit scalar, 1. By defining the operation of conjugation rather than inversion it is possible to do something even more useful, which is to maintain the property of the result being a metric-invariant scalar, but force it to correspond with what is known familiarly as the square modulus of the vector or, equally, of its conjugate covector. Much use can be made of this in the kinematical approximation to diffraction theory as discussed here. In conventional matrix representations conjugation corresponds simply to taking the transpose.

2. Representations of the incident beam, the scattering vector and the diffracted beam

Basic diffraction geometry is characterized by just three quantities: an incident photon, which suffers annihilation (*i.e.* 'dies'); a newly created radiant photon, usually described conveniently, but incorrectly, as 'scattered'; and a periodicity within the crystal, commonly referred to as 'Bragg planes' (Bragg, 1913). Rather remarkably, ever since the earliest days of X-ray diffraction, crystallographers have described all three quantities by apparently similar vectors in reciprocal space. The theory underlying this model is far too well established to warrant an exposition here.

It is convenient, and indeed usually necessary, when using vectorial methods to be able to represent algebraically at least some quantities in a left-acting and in a right-acting form. This choice of representation is certainly a necessity when discussing diffraction theory. Traditionally, row and column vectors of coefficients have been used to represent vector quantities, but these have some disadvantages; in particular: they are cumbersome

Table 1. *General symbol table* (*see Thomas*, 1990*a*)

$\cdot$	missing argument of a function
$\cdot\lceil\cdot$	the rotationally skew-symmetric operator
$\cdot\lfloor\cdot$	the inverse rotationally skew-symmetric operator
$\cdot\underline{\vert}\cdot$	plane projective operator equivalent in form to the rotationally symmetric operator
$\cdot\overline{\vert}\cdot$	plane projective operator equivalent in form to the rotationally antisymmetric operator
$\cdot\vert\cdot$	the rotationally invariant operator which projects onto the named axis
$\cdot\vert$	an intrinsically dimensionless quantity in vector formation, like a rotational axis operator
$\vert\cdot$	an intrinsically dimensionless quantity in covector formation, like a rotational sixa operator
$\vec{\cdot}$	a quantity like a pointer or a signed axis
$\cdot$	an angle of rotation
$\acute{\cdot}, \grave{\cdot}$	a rotation operator, and its inverse
$\lceil\cdot\rfloor$	a bidirectional unary skew operator replacing the conventional vector cross product
$\lfloor\cdot\rceil$	conjugate inverse to $\lceil\cdot\rfloor$; $\lfloor\cdot\rceil = -\lceil\cdot\rfloor$; $\lceil\cdot\rfloor \equiv \Vert\cdot\Vert\,\cdot\lceil\cdot$
$[\cdot]$	rounded to the nearest whole number
$\vert\cdot\vert$	the absolute value
$\Vert\cdot\Vert$	the Euclidean norm of a vector or covector
$\partial/\partial\cdot$	partial differentiation
$\nabla_{\cdot}\cdot$	alternative notation for partial differentiation
sd($\cdot$)	standard deviation
var($\cdot$)	variance
$\langle(\Delta\cdot)^2\rangle$	alternative notation for variance
$\lceil\cdot\rangle\langle\cdot - \bar{\cdot}\rangle\langle\bar{\cdot}\rceil$	variance–covariance of a vector variable
$\oplus$	addition in the sense that increases the absolute value of the result
$\otimes$	tensor outer product
$\wedge$	vector cross product; row vectors cross to row vectors, column vectors to column vectors
$\blacksquare$	correspondence or inner product; in component representation, $\mathbf{A}\blacksquare\mathbf{B} = A_i^j B_i^j$
$\forall_{\underline{\quad}}$	for all values of
$\bar{\quad}$	(overline) a generalized matrix inverse (Moore, 1920; Penrose, 1955); also arithmetic mean
$\widehat{\quad}$	(wide hat) implies the presence of a unit normalization
$\Rightarrow$	which implies
$\Longleftrightarrow$	which implies and is implied by
$\sim$	can be represented by
$\equiv$	equivalent
px	a pixel (a single picture element)

because one must write down three or six times more symbols than is really necessary; the resulting equations no longer display their behaviour, structure or symmetry clearly; the emphasis is placed on the value a given component has in a given representation or space, rather than on the physical quantity itself. Here, simple symbols such as $\langle$S and S$\rangle$ are used in preference to represent the incident beam as left- and right-multipliers. The symbols used in this section are listed in Table 2. The similarity of this notation to that used by Dirac (1958) is not accidental; the type of form that appears, for example, in (2.3), (3.3) or (7.1) is always immediately recognizable as a scalar, and the equations here will always remain true if flipped from left to right across the page, which corresponds to performing a transpose in matrix notation. However, there is a deeper underlying geometric interpretation which will start to become apparent shortly.

Whatever the precise definition of our notational symbols, it must always be possible to extract from them the values of the physical quantities they represent. Thus, by analogy with the conventional equation of physics for the energy of a photon: $E = cp = c\hbar k = c\hbar\|\mathrm{k}\|$, we can say (apart from an arbitrary factor) that we should be able to write

$$E = c\hbar\|\langle\mathrm{S}\| \quad \Longleftrightarrow \quad E = c\hbar\|\mathrm{S}\rangle\| \qquad (2.1)$$

if S$\rangle$ represents a photon. This demands that we can assign a unique scalar modulus to both left- and right-forms of symbols such as S$\rangle$:

$$\|\langle\mathrm{S}\| = \|\mathrm{S}\rangle\|. \qquad (2.2)$$

In fact, this modulus is vary rarely needed because $\langle$S and S$\rangle$ can be defined in such a way that they act on each other to produce the square modulus directly:

$$\langle\mathrm{SS}\rangle \quad (= \|\langle\mathrm{S}\|\,\|\mathrm{S}\rangle\|) \quad = \left(\frac{E}{c\hbar}\right)^2. \qquad (2.3)$$

Quantities which act on each other in this way must necessarily behave as a mutual covector–vector pair, but the

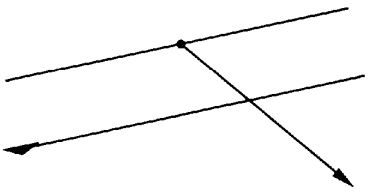

Fig. 2. The action of a covector upon a vector. Covectors are represented faithfully and naturally by a series of contour planes. Here, a free covector acting on a vector is represented by a downhill contour intersecting the tail of the vector and by an uphill contour one unit higher marked with a broad arrowhead. The value of the product is the number of contour levels between the head and the tail of the vector, which is $2\frac{1}{2}$ in the case illustrated. It is characteristic of this representation that larger covectors have their contours closer together. Perhaps it takes some time to accommodate this apparent perversity, but it is quite sensible when it is realized that it is the density of contour lines that is proportional to the magnitude of the covector.

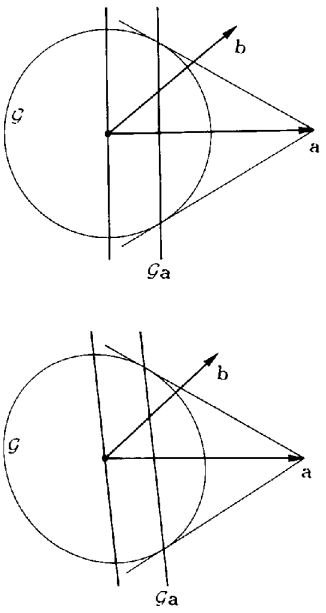

Fig. 3. The rigorous geometrical interpretation of a scalar (*i.e.* dot) product. This diagram shows a secure geometrical construction representing the scalar product of two vectors which necessarily involves the use of a metric tensor, $\mathcal{G}$, here represented by a circular contour on the left or (only apparently) by an elliptical contour on the right. The construction proceeds as follows: draw the unit circle representing the metric centred on the tail of one of the vectors, say a; then draw both tangents to the circle which meet the head of this vector; the line joining the two tangential points is the unit contour of the covector conjugate to this vector. The scalar product of this first vector with the second, say **b**, is then generated by allowing this constructed covector to act upon the second vector directly, in this case giving the value $2\frac{1}{2}$. The diagram on the right shows that this construction survives variations in the metric, which is not true of less rigorous definitions based upon the right-projection of one vector upon the other. When handled with proper regard for metric variability, the scalar product is thus seen to be more complicated than the action of a covector upon a vector as proposed in this paper. Indeed, the apparent simplicity of the scalar product is an artefact of always working in a Cartesian–Euclidean space.

complete symmetry of the equation means that both symbols must comprehend both properties. Nonetheless, it is often useful to regard ⟨S as a covector in reciprocal space and S⟩ as a vector in reciprocal space. These assignments are reversed in direct space. Some notational symmetries and correspondences with dual and Fourier spaces are discussed more fully in Appendix *A*.

It is a frequently used convention to demand that

$$\langle \mathrm{SS} \rangle = 1 \quad (\Rightarrow E = c\hbar) \tag{2.4}$$

which specifies the use of dimensionless reciprocal-lattice units.* For the purposes of the present discussion, and in many practical circumstances, the normalization implicit in this equation is not imposed; indeed, it is preferable not to do so to avoid the risk of making (2.3) appear to lose its meaning. However, when (2.4) has been imposed, the fact can be noted by placing a wide hat over the other equations which are sensitive to normalization, *e.g.* (7.1). Equation (2.4) also, rather inconveniently, has the side-effect of redefining both the scaling and dimensions of energy.

Clearly, when working in a Cartesian–Euclidean space with basis axes, x, y, z, and with the received conventions of matrix algebra, the forms

$$\langle \mathrm{S} \sim (S_x \quad S_y \quad S_z) \qquad \text{and} \qquad \mathrm{S}\rangle \sim \begin{pmatrix} S_x \\ S_y \\ S_z \end{pmatrix} \tag{2.5}$$

will be satisfactory computational representations for the character in reciprocal space of the more fundamental quantities, ⟨S and S⟩.

Importantly, a column is not necessarily associated with a vector and a row with a covector, as can be seen from the conjugational transposition of an equation which does not imply any geometrical change when the symbols involved comprehend both properties simultaneously. It is appropriate to remark, too, on the complete arbitrariness of row and column vectors at this point, for they are just a convention for placing resolved components on paper. Had history so dictated, we could just as well now be premultiplying matrices with column vectors and postmultiplying them with row vectors or, indeed, doing something completely different. Any sense of attachment to component representations can also be deprecated, for the components change if the chosen set of axes changes, and are thus also arbitrary. A notation like ⟨S or S⟩ should therefore be thought of as the primary geometrical representation of a physical quantity, rather than as a shorthand

* This is the 'egalitarian' photocentric view of the world, in that it appears to make all photons equal, but it is probably more useful as an *aide memoire* for the λ^{-4} dependence of Rayleigh scattering. The argument is that a photon has no means to measure the size of a scatterer other than by reference to its own wavelength, necessarily regarded as the unit of length. Thus, the perceived area of any given scatterer, say atmospheric molecules, necessarily comes out proportional to λ^{-2}. The amplitude of the scattering is proportional to this area providing that it is very small, but the intensity is amplitude squared, giving the well known λ^{-4} dependence responsible for the blue colour of the sky.

Table 2. *Symbol table for* §2

c	the speed of light
E	the energy of a photon
$\hbar$	Planck's constant
k	wavenumber, $\|\|\mathbf{k}\|\|$
k	a wave vector
p	modulus of momentum
S⟩, ⟨S	the periodic structure of minus the mean incident-beam wave vector, and its conjugate
S_x, S_y, S_z	Cartesian components in a reciprocal-space vector representation of S⟩ or ⟨S

for the capricious and purely conventional row and column vectors which can be used to represent the quantity computationally.

3. The diffraction condition

The diffraction of light was first discovered by Francesco Maria Grimaldi (1655), at some time between 1637 and 1654 (Westfall, 1980), but it was not until 1912 that the diffraction of X-rays was first observed by Laue (Laue, 1912; Friedrich, Knipping & Laue, 1912). The large body of analysis available to describe X-ray diffraction tends to occlude the simplest and most important physical principles involved: both energy and momentum must be conserved. In the absence of phonon coupling, these two alone can summarize the most important features of an X-ray diffraction experiment in the form of nothing more complicated than an isosceles triangle.

Following the conventions of the last section, the conservation of momentum can be represented in a very intuitive manner, either in direct space by covectors, or in reciprocal space by vectors [see equation (11.1) in *Goniometry*]:

$$\langle \mathrm{T} = \langle \mathrm{R} - \langle \mathrm{S} \qquad \Longleftrightarrow \qquad \mathrm{T}\rangle = \mathrm{R}\rangle - \mathrm{S}\rangle. \quad (3.1)$$

This is illustrated in Fig. 4.

It is important to realize that the formal derivation and interpretation of this simple equation are not actually trivial: in particular, it must be remembered that its most rigorous derivation comes from the balance of periodicities in space and in time; the interpretation in terms of momentum is a simplification justifiable only in terms of the physics of the present century. T⟩ and S⟩ refer to similar objects (two photons) and to fit into the equation we demand that R⟩ describes the crystal in a compatible way: thus we are forced to hold that $-$S⟩ is proportional to the momentum given to the new (scattered) photon by the (dying) incoming one, and that R⟩ is proportional to the momentum given to the new photon by the bulk crystal – the so-called 'crystal momentum'.

The equation representing conservation of energy during diffraction hides a further complication: the energy of a photon is classically given by $E = cp = c\hbar k$, but this formula is quite different to that of the classical kinetic energy of the crystal, which would be of the form $E = p^2/2m$, so the two enter the equation in a different way. However, the mass, m, of even the tiniest crystallite is so enormously large in comparison with the equivalent mass of the photons that the kinetic energy of the crystal can be ignored completely. We thus set the energies of the two photons to be equal, directly by setting $\|\mathrm{T}\rangle\| = \|\mathrm{S}\rangle\|$, but more conveniently by using symmetric quadratic forms proportional to E^2 [see equation (11.2) in *Goniometry*]:

$$\langle \mathrm{TT}\rangle = \langle \mathrm{SS}\rangle. \quad (3.2)$$

The inadvisability of imposing (2.4) always can be seen immediately, since it all but deprives the present equation of any meaning, the more especially when the incident X-rays are not exactly monoenergetic.

Direct substitution of (3.1) into (3.2), remembering that $\langle \mathrm{SR}\rangle \equiv \langle \mathrm{RS}\rangle$, gives the equation that we call the 'diffraction condition' [see equation (11.3) in *Goniometry*]:

$$\begin{aligned} \langle \mathrm{RR}\rangle - \langle \mathrm{SR}\rangle - \langle \mathrm{RS}\rangle \quad &\equiv \quad \langle \mathrm{RR}\rangle - 2\langle \mathrm{RS}\rangle \\ &\equiv \quad \langle \mathrm{RR}\rangle - 2\langle \mathrm{SR}\rangle = 0. \end{aligned} \quad (3.3)$$

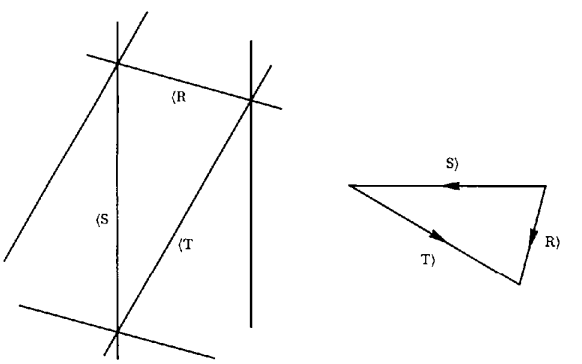

Fig. 4. Basic diffraction geometry as covectors or as vectors. The covector diagram on the left displays most clearly the balance of periodicities between ⟨S, ⟨T and ⟨R in direct space. The 'direction' or 'sign' of each covector is marked by the positioning of its label, which occupies the more positive side of an arbitrary contour [this is somewhat simpler than the method used by Burke (1985)]. The equivalent conjugate diagram (on the right) using vectors in reciprocal space is much more familiar. The vector, S⟩, is defined to point in the direction from the crystal to the source, and thus in the opposite direction to the motion of the photons. This choice is justified on several grounds: it is convenient to use the nominal crystal position as the origin for all quantities in direct space; the equations, fortuitously, have fewer minus signs; perhaps more importantly, there is a direct analogy with the analytical quantum-mechanical formula for the scattering event, where the incoming photon being destroyed and the newly created outgoing photon appear in mutually conjugated forms.

Table 3. *Symbol table for* §3 *et seq.*

$\mathbf{1}$	the multiplicative identity operator; representable by a unit matrix
$\langle$A, $\langle$B, $\langle\Psi$	basis covectors in the analysis of the diffraction angle
α	relates direct-space and reciprocal-space representations of a scattered beam
cos	the cosine function
ϵ	the symmetric form $\langle S\Psi\rfloor\Psi X\rangle = \langle X\Psi\rfloor\Psi S\rangle = -\langle S\Psi\lceil\Psi X\rangle = -\langle X\Psi\lceil\Psi S\rangle$
η	the antisymmetric form $\langle S\Psi\lceil\Psi X\rangle = \langle X\Psi\lceil\Psi S\rangle = -\langle S\Psi\rfloor\Psi X\rangle = -\langle X\Psi\rfloor\Psi S\rangle$
$\Theta\}$	direct-space representation of a scattered beam
$\mathbf{F}$	direct-space conventional unit cell; inverse of $\overline{\mathbf{F}}$; columns are conventional-lattice vectors
$\overline{\mathbf{F}}$	reciprocal-space conventional unit cell; inverse of $\mathbf{F}$; rows are reciprocal-lattice vectors
h	Miller indices, (h, k, ℓ)
L	a generalized form of the Lorentz factor; conventional form is $\lvert\widehat{L}\rvert$; see Υ below
l, m, n	direction cosines
m	mass
Q	a point on a detector faceplate, (Q_Y, Q_Z)
R$\rangle$, $\langle$R	the periodic structure of a Bragg plane in the diffracting position, and its conjugate
ρ	the symmetric form $\langle S\Psi\rfloor\Psi R\rangle = \langle R\Psi\rfloor\Psi S\rangle$
sin	the sine function
T$\rangle$, $\langle$T	the periodic structure of the scattered-beam wave vector, and its conjugate
X$\rangle$, $\langle$X	the periodic structure of a Bragg plane (referred to the crystal frame), and its conjugate
ξ	the conventional radial variable used in the rotation method (Arndt & Wonacott, 1977)
y	the antisymmetric form $\langle S\Psi\lceil\Psi R\rangle = \langle R\Psi\lceil\Psi S\rangle = -\langle R\Psi\rfloor\Psi S\rangle = -\langle S\Psi\rfloor\Psi R\rangle$
Υ	the antisymmetric form $\langle S\Phi\lceil\Phi R\rangle = \langle R\Phi\lceil\Phi S\rangle = -\langle R\Phi\rfloor\Phi S\rangle = -\langle S\Phi\rfloor\Phi R\rangle = L^{-1}$
ϕ	a very small perturbation in the diffraction angle (about $\vec{\Phi}$)
$\vec{\Phi}$	a signed representation of the instantaneous axis of rotation (*i.e.* axis of angular velocity)
$\dot{\mathbf{\Phi}}$	rotation through ϕ about $\vec{\Phi}$
$\Phi\vert\Phi, \Psi\vert\Psi$	the diffraction-angle invariant operators
$\Phi\lceil\Phi, \Psi\lceil\Psi$	the diffraction-angle skew-symmetric operators
$\Phi\rfloor\Phi, \Psi\rfloor\Psi$	the inverse diffraction-angle skew-symmetric operators
$\Phi\perp\Phi, \Psi\perp\Psi$	the diffraction-angle symmetric operators
ψ	the (Arndt–Wonacott) diffraction angle (about $\vec{\Psi}$)
$\vec{\Psi}$	a signed representation of the axis of total rotation from datum
$\dot{\mathbf{\Psi}}, \grave{\mathbf{\Psi}}$	rotation through ψ about $\vec{\Psi}$, and its inverse

If S$\rangle$ is held fixed, this is the equation of the Ewald sphere (Ewald, 1913); if R$\rangle$ is held fixed, it is the equation of the 'diffraction plane', which bisects the vector representing R$\rangle$ in reciprocal space. The important consequences of holding T$\rangle$ fixed are the subject matter of another paper (Thomas, 1992*a*).

Very frequently, a crystal is turned until a given reciprocal-lattice point is in the diffraction condition. If X$\rangle$ is used to denote the reciprocal-lattice point in some datum orientation of the crystal, then it is always possible to write

$$\langle R = \langle X\grave{\mathbf{\Psi}} \qquad \Longleftrightarrow \qquad R\rangle = \dot{\mathbf{\Psi}}X\rangle, \tag{3.4}$$

where $\dot{\mathbf{\Psi}}$ is an operator describing the rotation of the crystal from the position at which $\psi = 0$, and $\grave{\mathbf{\Psi}}$ is its inverse. Table 3 gives a list of symbols for this and the following sections. The definition of $\dot{\mathbf{\Psi}}$ follows that in *Goniometry*, and expands to

$$\dot{\mathbf{\Psi}} = \Psi\vert\Psi + \Psi\lceil\Psi \sin\psi + \Psi\rfloor\Psi \cos\psi, \tag{3.5}$$

which substitutes into (3.4), itself substituted into (3.3). A trivial cancellation of $\grave{\mathbf{\Psi}}\dot{\mathbf{\Psi}} = \mathbf{1}$ and division by 2 gives the following fundamental equation for the diffraction angle:

$$\frac{\langle XX\rangle}{2} - \langle S\Psi\vert\Psi X\rangle - \langle S\Psi\lceil\Psi X\rangle \sin\psi - \langle S\Psi\rfloor\Psi X\rangle \cos\psi = 0. \tag{3.6}$$

This equation is most commonly interpreted in terms of the rotation camera, when ψ is known as the Arndt–Wonacott angle, but is intrinsically completely general, $\vec{\Psi}$ being any axis of total rotation from datum.

The derivatives of R$\rangle$ are important during the refinement of experimental parameters, when they couple into the normal equations of least-squares-minimization procedures by the chain rule of differential calculus. Only two derivatives of (3.4) are commonly used, which are

$$\nabla_{X\rangle} R\rangle = \dot{\mathbf{\Psi}} \tag{3.7}$$

and

$$\nabla_{\psi} R\rangle = \nabla_{\psi}\dot{\mathbf{\Psi}}X\rangle = \Psi\lceil\Psi\dot{\mathbf{\Psi}}X\rangle = \Psi\lceil\Psi R\rangle. \tag{3.8}$$

This latter form has already been seen, embedded in

(11.1) of *Goniometry*. Another derivative with respect to changes in the orientation of the total rotation axis could also be defined, but has so far found no application. Much more useful, though, is to consider the effects of a very small extra rotation about an axis, say $\vec{\Phi}$, not generally the same as that of the total rotation from datum, $\vec{\Psi}$. Calling the angle of this extra rotation ϕ and treating it as variable but asymptotically zero, $\phi \rightarrow 0$, so that $\dot{\boldsymbol{\Phi}} \rightarrow \mathbf{1}$, whilst ψ is held to be temporarily constant enables the replacement

$$\dot{\boldsymbol{\Psi}} \longrightarrow \dot{\boldsymbol{\Phi}}\dot{\boldsymbol{\Psi}} \tag{3.9}$$

and (3.8) can be replaced by the more general

$$\nabla_\phi \mathrm{R}\rangle = \nabla_\phi \dot{\boldsymbol{\Phi}}\dot{\boldsymbol{\Psi}}\mathrm{X}\rangle = \Phi\rfloor\Phi\dot{\boldsymbol{\Phi}}\dot{\boldsymbol{\Psi}}\mathrm{X}\rangle \rightarrow \Phi\rfloor\Phi\dot{\boldsymbol{\Psi}}\mathrm{X}\rangle = \Phi\rfloor\Phi\mathrm{R}\rangle. \tag{3.10}$$

This shows rather spectacularly that the most general case has equations of exactly the same form as those for the rotation method, the only difference being that when the symbol $\Psi\rfloor\Psi$ appears as the equivalent of the derivative with respect to the diffraction angle, ∇_ψ, it must be replaced by $\Phi\rfloor\Phi$. The operator $\dot{\boldsymbol{\Psi}}$ representing total rotation is unaffected so long as the equations are evaluated at $\phi = 0$, which is always possible. A rather helpful way to view the equations is to observe that $\dot{\boldsymbol{\Psi}}$ represents the transformation of reference axes between the current crystal position and its datum position, whilst $\Phi\rfloor\Phi$ picks out the instantaneous effects of the motion of the crystal. Clearly, on a rotation camera proper, $\vec{\Phi}$ and $\vec{\Psi}$ are synonymous and ϕ can differ from ψ only by shift of origin.

The reciprocal-lattice vector, $\mathrm{X}\rangle$, used above is defined in terms of the Miller indices, h, and the conventional reciprocal unit cell at datum, $\overline{\mathbf{F}}$ [equivalent to the transpose of **UB** in Busing & Levy (1967)], by

$$\begin{aligned}\langle \mathrm{X} = \langle \mathrm{h}\overline{\mathbf{F}} &= (h,k,\ell)\begin{pmatrix}\langle^h\overline{\mathrm{F}}\\ \langle^k\overline{\mathrm{F}}\\ \langle^\ell\overline{\mathrm{F}}\end{pmatrix}\\ &\sim (h,k,\ell)\begin{pmatrix}{}^h\overline{F}_x & {}^h\overline{F}_y & {}^h\overline{F}_z\\ {}^k\overline{F}_x & {}^k\overline{F}_y & {}^k\overline{F}_z\\ {}^\ell\overline{F}_x & {}^\ell\overline{F}_y & {}^\ell\overline{F}_z\end{pmatrix}\\ &= (X_x \quad X_y \quad X_z).\end{aligned} \tag{3.11}$$

It will be seen that $\overline{\mathbf{F}}$ splits naturally into rows representing direct-space covectors or reciprocal-space vectors, here written such that $\langle^h\overline{\mathrm{F}}$ corresponds directly with the conventional reciprocal-lattice vector $\mathbf{a}^{*\mathrm{T}}$, $\langle^k\overline{\mathrm{F}}$ with $\mathbf{b}^{*\mathrm{T}}$ and $\langle^\ell\overline{\mathrm{F}}$ with $\mathbf{c}^{*\mathrm{T}}$. The differential of $\langle\mathrm{X}$ with respect to $\overline{\mathbf{F}}$ can be written conveniently in contracted symbolic form as

$$\nabla_{\overline{\mathbf{F}}}\langle\mathrm{X} = \mathrm{h}, \tag{3.12}$$

which is just about as simple as it could be, though perhaps it displays its computational structure more clearly when expanded slightly into

$$\begin{aligned}\frac{\partial\langle\mathrm{X}}{\partial\langle^h\overline{\mathrm{F}}} &= h \equiv h\mathbf{1},\\ \frac{\partial\langle\mathrm{X}}{\partial\langle^k\overline{\mathrm{F}}} &= k \equiv k\mathbf{1},\\ \frac{\partial\langle\mathrm{X}}{\partial\langle^\ell\overline{\mathrm{F}}} &= \ell \equiv \ell\mathbf{1}.\end{aligned} \tag{3.13}$$

The trivial expansion of these vector derivatives of vectors into a matrix form serves only to satisfy the accepted convention that the result should be a matrix form; that the simpler scalar form is possible is an indication of the fact that $\langle\mathrm{X}$, $\langle^h\overline{\mathrm{F}}$, $\langle^k\overline{\mathrm{F}}$, $\langle^\ell\overline{\mathrm{F}}$ are all defined on the same metric which consequently vanishes from the result. The natural placement of the putative small shifts in the (transposed) unit-cell vectors is on the left-hand side of these derivatives, though this shifts to the right-hand side of the scalar Miller indices in conventional component representations. These derivatives couple $\overline{\mathbf{F}}$ directly to $\langle\mathrm{X} \equiv \mathrm{X}\rangle$ and hence to calculated spot positions using the chain rule of the differential calculus, so they enable $\overline{\mathbf{F}}$ to be refined from the observations.

4. Detector geometry

It has been traditional for every film or detector geometry to be analysed using its own special coordinates and system of equations, often with considerable ensuing confusion and inconvenience. Examples which can be cited are: the film axes, Y_F and Z_F, used by Arndt & Wonacott (1977, p. 82) for the rotation camera, which do not translate into the detector axes, Y and Z, of its electronic successor, the Enraf–Nonius FAST system; the confusingly similar axes used by Klinger & Kretsinger (1989); the angular detector coordinates, γ and ν, used on some cylindrical neutron area detectors (Stansfield, 1983) or the ordinary spherical coordinates, θ and ϕ, used for a similar purpose in some analyses of the shape of diffraction spots (Roth & Lewit-Bentley, 1986). Other specialized applications lead to further definitions of angles (*cf. inter alia* Schwarzenbach & Flack, 1989). This diversity of representation is unnecessary, since the vast majority of X-ray area detectors can be represented adequately† by a 'plane of detection', either real or assumed. This can be defined and described by a unified mathematical structure based on three bound vectors (Thomas, 1986*c*) or, equivalently, the three conjugate covectors. The most basic vectorial description is based on the vectors d^Y, d^Z and d^O. The symbol definitions for this section are given in Table 4.

† The representation ceases to be adequate when analysing the profiles of diffraction spots across the plane of detection if the convergence or divergence of the scattered beams is such that the shape is materially different in the real detection region from that in the assumed region. This problem never occurs with a flat solid-state detector like that in the FAST system, in film or in a phospholuminescent imaging plate, but it can be quite severe for thick drift chambers with focusing optics.

Table 4. *Symbol table for* §4

$\mathbf{B}$	(Beta) the set of detector-corner positions (or beta-lights on the FAST system)
B_n	(Beta) the position of the nth detector corner, written computationally as a column vector
B_{ni}	(Beta) the ith component of a Cartesian representation of B_n
Γ	the formal name of the calibration-grid geometry transformation (Thomas, 1989)
$\mathbf{d}$	the set of detector vectors, interpretable as a matrix, $[\mathrm{d}^Y\ \mathrm{d}^Z\ \mathrm{d}^O]$
$\mathrm{d}^I, \mathrm{d}^O$	vectors describing the geometry of the detection plane, written computationally as column vectors
${}^I\mathrm{d}$	transposes of d^I, written computationally as a row vector
$\mathrm{d}^\perp$	auxiliary vector from the crystal to the detector, meeting the detector plane perpendicularly
$\mathbf{d}'$	the set of image vectors
$\mathrm{d}'^I, \mathrm{d}'^O$	vectors describing the geometry of the image plane; $\mathrm{d}'^O = \mathrm{d}^O$
$\mathbf{D}$	the set of detector covectors, interpretable as the matrix inverse to $\mathbf{d}$
${}^I\mathrm{D}$	a bound covector delineating the detector I coordinate, written computationally as a row vector
D^I	transpose of ${}^I\mathrm{D}$, written computationally as a column vector
${}^\parallel\mathrm{D}, \mathrm{D}^\parallel$	a bound covector describing the detector plane, and its transpose
$\mathbf{D}'$	the set of image covectors, interpretable as the matrix inverse to $\mathbf{d}'$
${}^I\mathrm{D}', \mathrm{D}'^I$	a bound covector delineating the image I coordinate, and its transpose
${}^\parallel\mathrm{D}', \mathrm{D}'^\parallel$	a bound covector describing the image plane, and its transpose; ${}^\parallel\mathrm{D}' = {}^\parallel\mathrm{D}$
I	either Y or Z
j	number and dummy index, usually associated with Y components
k	number and dummy index, usually associated with Z components
μ_{Ijk}	coefficients of the M transformation (Thomas, 1989)
M	(Mu) the formal name of the monitorable short-term distortion transformation (Thomas, 1989)
O	label for the origin of the detector coordinates
x, y, z	the labels of the laboratory axes
Y	the label for the first of the detector faceplate axes (usually vertical)
Z	the label for the second of the detector faceplate axes (usually horizontal)

The bound vector from the nominal crystal position to the point on the detector plane that we wish to call the origin is called d^O. It is not necessarily perpendicular to the plane of detection. These vectors follow the same type of notational convention whereby a left to right flip, in this case of the subsidiary label and the main symbol, denotes the conjugate transpose. The Dirac-like brackets are thus not used, being unnecessary, and can be reserved for reciprocal-space usage. The axes of images collected with X-ray area diffractometers [*e.g.* FAST systems (uniquely at the time of writing)] are conventionally called Y and Z, and it is convenient to use the same nomenclature also for cameras [*e.g.* multiwire proportional counters (MWPCs), film and phospholuminescent imaging plates (PIPs)]. Then the direction and scaling of the dimensionless detector-plane coordinates, (Q_Y, Q_Z), are defined by the vectors d^Y and d^Z. Typically, but not necessarily, d^Y and d^Z are mutually perpendicular and have equal lengths of 1 mm. The three vectors can be combined to form the basic direct-space description of the detection plane as a single algebraic symbol with the computational structure of a 3×3 matrix:

$$\mathbf{d} = \left[\mathrm{d}^Y\ \mathrm{d}^Z\ \mathrm{d}^O\right] \sim \begin{bmatrix} d_x^Y & d_x^Z & d_x^O \\ d_y^Y & d_y^Z & d_y^O \\ d_z^Y & d_z^Z & d_z^O \end{bmatrix}. \tag{4.1}$$

Many calculations of detector geometry involve the matrix inverse to $\mathbf{d}$, called $\mathbf{D}$, having the structure of a triplet of covectors, ${}^Y\mathrm{D}$, ${}^Z\mathrm{D}$ and ${}^\parallel\mathrm{D}$:

$$\mathbf{D} = \begin{bmatrix} {}^Y\mathrm{D} \\ {}^Z\mathrm{D} \\ {}^\parallel\mathrm{D} \end{bmatrix} \sim \begin{bmatrix} {}^YD_x & {}^YD_y & {}^YD_z \\ {}^ZD_x & {}^ZD_y & {}^ZD_z \\ {}^\parallel D_x & {}^\parallel D_y & {}^\parallel D_z \end{bmatrix}. \tag{4.2}$$

We must have here (by definition) $\mathbf{Dd} = \mathbf{1}$, where $\mathbf{1}$ is the multiplicative identity operator, which expands to the 3×3 unit matrix. The vectors and covectors defining $\mathbf{d}$ and $\mathbf{D}$ suffice for calculations of diffraction geometries, but an extra vector, perpendicular to the plane of the detector, appears in calculations of the illumination during calibration procedures [Thomas, 1990*b*, equation (4.3)]. This vector is called $\mathrm{d}^\perp$, and it is given by

$$\mathrm{d}^\perp = \mathrm{D}^\parallel|^\parallel\mathrm{D}\,\mathrm{d}^O \sim \frac{\mathrm{d}^Y \wedge \mathrm{d}^Z\ \ {}^Z\mathrm{d} \wedge {}^Y\mathrm{d}}{{}^Z\mathrm{d} \wedge {}^Y\mathrm{d}\ \ \mathrm{d}^Y \wedge \mathrm{d}^Z}\,\mathrm{d}^O \tag{4.3}$$

where the vertical line between $\mathrm{D}^\parallel$ and ${}^\parallel\mathrm{D}$ denotes the action of the rotationally invariant operator defined in *Goniometry* and generically written as $\cdot|\cdot$. (The fraction has the computational structure of an outer product of column vector times row vector, all divided by the inner product of row vector times column vector, making an operator representable as a deponent 3×3 matrix.) Equation (4.3) also exposes the connection in three-dimensional space between a covector and a bivector composed from two vectors lying in a contour plane characterizing the covector.

It is often even more convenient to map the image of the diffraction pattern on the detector faceplate onto a dimensionless unit square (Thomas, 1989), and a similar set of 'image vectors', d'^{Y}, d'^{Z}, d'^{O}, is appropriate for handling the result of this transformation. On the Enraf–Nonius FAST system, the corners of the unit square are deliberately chosen so that they align with the positions of the four beta-lights, which are small radioactively excited light sources tucked away in the occluded corners of the snub-rectangular faceplate (see Fig. 5). The equations of this section can accommodate any detector, simply by defining a fixed rectangle over the imaging area; the four corners of the rectangle then assume the rôle of B_0, B_1, B_2 and B_3 on the FAST system.

The matrix of image vectors, $\mathbf{d}'$, is best defined indirectly as the inverse of the matrix of conjugate covectors, $\mathbf{D}'$, which is defined to satisfy

$$\mathbf{D}'\mathbf{B} = \begin{bmatrix} {}^{Y}\mathrm{D}' \\ {}^{Z}\mathrm{D}' \\ {}^{\|}\mathrm{D}' \end{bmatrix} [\mathrm{B}_0 \quad \mathrm{B}_1 \quad \mathrm{B}_2 \quad \mathrm{B}_3] = \begin{bmatrix} -1 & +1 & +1 & -1 \\ -1 & -1 & +1 & +1 \\ 1 & 1 & 1 & 1 \end{bmatrix} \tag{4.4}$$

where

$$\mathbf{B} = [\mathrm{B}_0 \quad \mathrm{B}_1 \quad \mathrm{B}_2 \quad \mathrm{B}_3] \sim \begin{bmatrix} B_{0x} & B_{1x} & B_{2x} & B_{3x} \\ B_{0y} & B_{1y} & B_{2y} & B_{3y} \\ B_{0z} & B_{1z} & B_{2z} & B_{3z} \end{bmatrix} \tag{4.5}$$

describes the positions of all four detector corners (or beta-lights). The (direct-space) bound vectors in $\mathbf{B}$ use the nominal crystal position as the origin. Equation (4.4) can, of course, be satisfied exactly only if $\mathbf{B}$ describes a parallelogram, but the usual rectangular geometry assures this. Explicitly,

$$\mathbf{D}' = \begin{bmatrix} {}^{Y}\mathrm{D}' \\ {}^{Z}\mathrm{D}' \\ {}^{\|}\mathrm{D}' \end{bmatrix} = \begin{bmatrix} -1 & +1 & +1 & -1 \\ -1 & -1 & +1 & +1 \\ 1 & 1 & 1 & 1 \end{bmatrix} \overline{[\mathrm{B}_0 \quad \mathrm{B}_1 \quad \mathrm{B}_2 \quad \mathrm{B}_3]} \tag{4.6}$$

where the overline denotes a generalized matrix inverse (Moore, 1920; Penrose, 1955; Appendix *B*); therefore

$$\begin{aligned} [\mathrm{d}'^{Y} \quad \mathrm{d}'^{Z} \quad \mathrm{d}'^{O}] &= \mathbf{d}' = \overline{\mathbf{D}'} \\ &= [\mathrm{B}_0 \quad \mathrm{B}_1 \quad \mathrm{B}_2 \quad \mathrm{B}_3] \overline{\begin{bmatrix} -1 & +1 & +1 & -1 \\ -1 & -1 & +1 & +1 \\ 1 & 1 & 1 & 1 \end{bmatrix}} \\ &= \frac{1}{4} [\mathrm{B}_0 \quad \mathrm{B}_1 \quad \mathrm{B}_2 \quad \mathrm{B}_3] \begin{bmatrix} -1 & -1 & 1 \\ +1 & -1 & 1 \\ +1 & +1 & 1 \\ -1 & +1 & 1 \end{bmatrix} . \end{aligned} \tag{4.7}$$

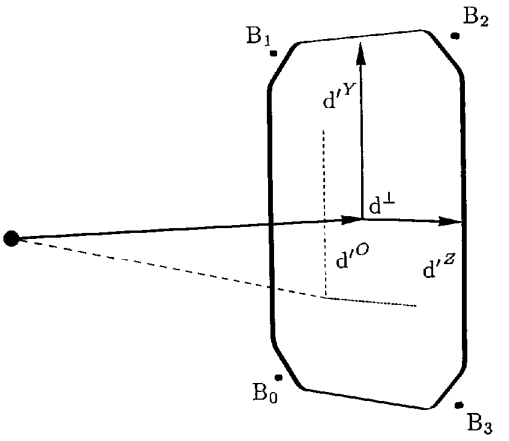

Fig. 5. The various vectors to describe image or detector geometry. Three vectors, **d**, labelled O, Y, Z are used to define the origin of image or detector coordinates; $\mathrm{d}'^{O} = \mathrm{d}^{O}$ defines the origin in the assumed detection plane and d'^{Y} and d'^{Z} define the principal axes of the dimensionless image coordinates. This geometry provides a completely general description of any plane detector, or any that can be represented adequately by an assumed plane of detection. This is usually possible, even for spherical detectors, with compensating modifications elsewhere (*e.g.* in the spatial-distortion calculations). The vector $\mathrm{d}^{\perp}$ is by definition always exactly perpendicular to the assumed plane of detection. The origin vector, $\mathrm{d}'^{O} = \mathrm{d}^{O}$, is often in very close alignment with $\mathrm{d}^{\perp}$; this is not necessarily the case, however, and an illustrative alternative is shown in broken lines. The labels d'^{O}, d'^{Y} and d'^{Z} which apply equally to the normal position of the vectors shown with continuous lines and to the unusual illustrative position in broken lines are deliberately placed in an intermediate position to indicate this fact.

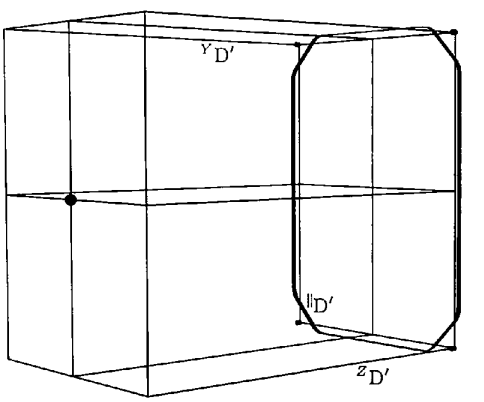

Fig. 6. The covectors used to describe image or detector geometry, laid over the outline of a detector. Covectors act on vectors to produce a scalar result; they are thus naturally representable as contour planes. Here, each of the three covectors is represented by its null contour and by its (labelled) unit contour. If $\mathrm{d}'^{O} = \mathrm{d}^{O}$ were to swing, ${}^{Y}\mathrm{D}'$ and ${}^{Z}\mathrm{D}'$ would too, so that their line of intersection remains always along d^{O}; ${}^{\|}\mathrm{D}'$ would be invariant as long as d^{O} remained in the originally defined plane of detection. Despite the analytical rigour and, indeed, convenience of using covectors, it must be admitted that they are much harder to illustrate in more than two dimensions, and the drawings are less easy to interpret. Fortunately, in an invariant Cartesian–Euclidean space, it is always possible to use the conjugate vectors, at the expense of implicitly making use of some right-angle constructions.

This equation interpolates in a reasonable manner if the positions B_0, B_1, B_2, B_3 are subject to small errors. Efficient calculations of the position that a photon will strike the detector using the quantities just defined are given in §5. The covectors in $\mathbf{D}'$ are illustrated in Fig. 6. Although they are associated with the unit square, which is dimensionless, the vectors in $\mathbf{d}'$ are still dimensioned as length, just like those in $\mathbf{d}$.

The similarity of the structure of this latter system of equations to, say, the system 4.4 (which models the spatial distortions of an area detector) in Thomas (1989), is hardly accidental, since d'^{Y}, d'^{Z}, d'^{O}, are functionally similar to the terms μ_{I10}, μ_{I01}, μ_{I00} respectively of the M transformation (which accommodates instabilities and variations in the imaging geometry). However, there is no counterpart to μ_{I11}, since the fixed Γ transformation being bypassed has no curvature.

Kahn (1986) has developed a modification of some of the equations of this section as first presented at the EEC Cooperative Workshop on Position-Sensitive Detector Software in Paris (see Thomas, 1986*c*) which neatly incorporates the major spatial distortion of the gas chamber at LURE, but inevitably loses the generality.

5. The position at which a photon strikes the detector

To calculate the position that a diffracted photon strikes the detector, it is necessary only to demand that the direct-space representation of the scattered beam, $\Theta\}$ (emanating from a position assumed to be at the centre of the crystal), be parallel to the reciprocal-space representation of the scattered beam, $\mathrm{T}\rangle$:

$$\Theta\} \equiv (\mathrm{d}^{Y} \quad \mathrm{d}^{Z} \quad \mathrm{d}^{O}) \begin{pmatrix} Q_Y \\ Q_Z \\ 1 \end{pmatrix} = (\mathrm{d}'^{Y} \quad \mathrm{d}'^{Z} \quad \mathrm{d}'^{O}) \begin{pmatrix} Q'_Y \\ Q'_Z \\ 1 \end{pmatrix} = \alpha \mathrm{T}\rangle. \quad (5.1)$$

The constant of proportionality, α, has the dimensions of area and $\mathrm{T}\rangle$ follows from (3.1), (3.4) and (3.9). The other symbols in this equation follow the notation in *Goniometry* and in Thomas (1989, 1990*b*) except that $\Theta\}$ here corresponds to Q^{*} in the papers on the calibration of area detectors. The curly brace is used to denote a direct-space vector specifically bound to the crystal. The preferred use of Θ in this context arises from the close relationship that the direct-space scattered beam bears to the θ arm of a classical diffractometer. Taking advantage of the relationships $\mathbf{Dd} = \mathbf{1}$ or $\mathbf{D}'\mathbf{d}' = \mathbf{1}$, one can rearrange these equations as

$$\begin{pmatrix} Q_Y \\ Q_Z \\ 1 \end{pmatrix} = \alpha \mathbf{D}\mathrm{T}\rangle = \alpha \begin{bmatrix} {}^{Y}\mathrm{D} \\ {}^{Z}\mathrm{D} \\ \|\mathrm{D} \end{bmatrix} \mathrm{T}\rangle$$

or

$$\begin{pmatrix} Q'_Y \\ Q'_Z \\ 1 \end{pmatrix} = \alpha \mathbf{D}'\mathrm{T}\rangle = \alpha \begin{bmatrix} {}^{Y}\mathrm{D}' \\ {}^{Z}\mathrm{D}' \\ \|\mathrm{D}' \end{bmatrix} \mathrm{T}\rangle \quad (5.2)$$

whence α can be eliminated and the solutions become simply the dimensionless ratios

$$Q_I = \frac{{}^{I}\mathrm{DT}\rangle}{\|\mathrm{DT}\rangle} \quad \text{or} \quad Q'_I = \frac{{}^{I}\mathrm{D}'\mathrm{T}\rangle}{\|\mathrm{D}'\mathrm{T}\rangle}, \quad (5.3_I)$$

where I represents either Y or Z. It should be noted that whilst both numerator and denominator in these equations individually result computationally in a single number which would often be called (imprecisely) a scalar, this number is manifestly not metric invariant. It is here, perhaps most clearly, that the significance of metric variations becomes most obvious: the usual convention is that reciprocal-space vectors are measured in inverse X-ray Å units, whilst the detector covectors are measured in inverse mm, which units differ by an immodest experimentally determined factor usually taken to be exactly 10^7. In the strictest definitions of modern geometry, only numbers which are also strictly metric invariant would be called scalars, but we lack the language (or indeed the patience) to make the distinction more generally. However, it is to be hoped that the deliberate difference in notations for vectors in reciprocal space and in direct space will be found helpful in maintaining this distinction. It might also be noted that this formula for Q is identical to the perspective projection of $\mathrm{T}\rangle$ onto the plane of the detector, taking the crystal as the eye-point. The formulae (5.3) for Q' are called the gamma-bypass transformation, because they circumvent the Γ transformation, which is part of the cascaded description of the spatial distortions of an area detector. [*Cf.* equations (2.1) and (2.2) in Thomas (1989).] They are used during high-speed calculations because overall they involve less computation.

Equivalent equations are available using the detector or image vectors rather than the covectors, by expanding $\mathbf{D}$ or $\mathbf{D}'$ in full as the matrices inverse to $\mathbf{d}$ or $\mathbf{d}'$ and cancelling the determinants:

$$Q_Y = \frac{{}^{Z}\mathrm{d} \wedge {}^{O}\mathrm{d}\ \mathrm{T}\rangle}{{}^{Y}\mathrm{d} \wedge {}^{Z}\mathrm{d}\ \mathrm{T}\rangle} \quad \text{or} \quad Q'_Y = \frac{{}^{Z}\mathrm{d}' \wedge {}^{O}\mathrm{d}'\ \mathrm{T}\rangle}{{}^{Y}\mathrm{d}' \wedge {}^{Z}\mathrm{d}'\ \mathrm{T}\rangle} \quad (5.4_Y)$$

and

$$Q_Z = \frac{{}^{O}\mathrm{d} \wedge {}^{Y}\mathrm{d}\ \mathrm{T}\rangle}{{}^{Y}\mathrm{d} \wedge {}^{Z}\mathrm{d}\ \mathrm{T}\rangle} \quad \text{or} \quad Q'_Z = \frac{{}^{O}\mathrm{d}' \wedge {}^{Y}\mathrm{d}'\ \mathrm{T}\rangle}{{}^{Y}\mathrm{d}' \wedge {}^{Z}\mathrm{d}'\ \mathrm{T}\rangle}. \quad (5.4_Z)$$

These coordinates are thinly disguised ratios of triple scalar products.

The derivatives of Q' are clearly useful for refinement purposes and are best expressed in terms of the defining covectors in $\mathbf{D}'$. With respect to $\mathrm{T}\rangle$ we have directly after a trivial rearrangement of the 'scalar' terms to emphasize the necessarily covector-like properties:

$$\nabla_{\mathrm{T}\rangle} Q'_I = \frac{\langle \mathrm{TD}'\| \ {}^{I}\mathrm{D}' - \langle \mathrm{TD}'^{I} \ \|\mathrm{D}'}{\langle \mathrm{TD}'\| \quad \|\mathrm{D}'\mathrm{T}\rangle}, \quad (5.5_I)$$

which is easily related to both $\mathrm{R}\rangle$ and $\mathrm{S}\rangle$ by the chain rule using $\nabla_{\mathrm{R}\rangle}\mathrm{T}\rangle = \nabla_{\mathrm{T}\rangle}\mathrm{R}\rangle = \mathbf{1}$ and $\nabla_{\mathrm{S}\rangle}\mathrm{T}\rangle = \nabla_{\mathrm{T}\rangle}\mathrm{S}\rangle = -\mathbf{1}$. It

would, however, be inconceivable that, on a machine of the precision and accuracy of a FAST system , the defining covectors within $\mathbf{D}'$ should be refined from diffraction data,* but on less accurate machines, or where there is a suspicion that a misalignment has been induced, the following derivatives with respect to the covectors might be found useful:

$$\nabla_{\mathrm{T}\mathbf{D}'} Q'_I = \frac{\mathrm{T}\rangle}{\|\mathbf{D}'\mathrm{T}\rangle} \tag{5.6$_I$}$$

and

$$\nabla_{\|\mathbf{D}'} Q'_I = -\frac{\mathrm{T}\rangle\langle\mathrm{TD}'^I}{\langle\mathrm{TD}'\|\ \|\mathbf{D}'\mathrm{T}\rangle}. \tag{5.7$_I$}$$

The putative small shifts in the covectors by which these latter two equations have been differentiated naturally premultiply rather than postmultiply the derivative forms.

6. The geometry of the rotation method and the diffraction angle

A contracted solution to the generalized equation of the Arndt–Wonacott diffraction angle was given in *Goniometry*, and the treatment here both formalizes the earlier exposition and extends it, by giving the explicit calculations of the terms ρ, y and $\mathrm{R}\rangle$.† First, three basis covectors with symmetrical properties related to the rotation axis and to the incident beam are defined (see Fig. 7):

$$\langle\mathrm{A} = \langle\mathrm{S}\Psi\rfloor\Psi, \tag{6.1}$$

$$\langle\mathrm{B} = \langle\mathrm{S}\Psi\lfloor\Psi, \tag{6.2}$$

$$\langle\Psi \equiv |\Psi \equiv \vec{\Psi}. \tag{6.3}$$

The notation here was described fully in *Goniometry*, but recapitulating, the *sixa*, $|\Psi$, here represents specific orbital planes of points turning on the ψ axis and $\langle\Psi$ is a covector representation of these. Computationally, $\langle\Psi$ would almost invariably be represented by a row vector of direction cosines aligned along the ψ axis.

The covectors in the last three equations are mutually orthogonal; $\langle\mathrm{A}$ and $\langle\mathrm{B}$ necessarily have the same modulus, but the modulus of $\langle\Psi$ need not be the same. (Indeed, it is more than likely that $\langle\Psi$ would even be dimensioned differently.) Thus the unrotated reciprocal-lattice vector can be resolved into the three components:

$$\begin{pmatrix}\epsilon\\ \eta\\ \zeta\end{pmatrix} = \begin{pmatrix}\langle\mathrm{A}\\ \langle\mathrm{B}\\ \langle\Psi\end{pmatrix}\mathrm{X}\rangle = \begin{pmatrix}\langle\mathrm{S}\Psi\rfloor\Psi\mathrm{X}\rangle\\ \langle\mathrm{S}\Psi\lfloor\Psi\mathrm{X}\rangle\\ \langle\Psi\mathrm{X}\rangle\end{pmatrix}, \tag{6.4}$$

which have distinctly different behaviours with respect to the angle of rotation, as expounded in *Goniometry*. For heuristic purposes only, this component representation is now rotated through the unknown ψ into a diffracting position using an archetypical 3×3 rotation matrix, giving the new component representation

$$\begin{pmatrix}\rho\\ y\\ \zeta\end{pmatrix} = \begin{pmatrix}\cos\psi & \sin\psi & 0\\ -\sin\psi & \cos\psi & 0\\ 0 & 0 & 1\end{pmatrix}\begin{pmatrix}\epsilon\\ \eta\\ \zeta\end{pmatrix}. \tag{6.5}$$

Direct expansion using the definitions of η and ϵ above shows that ρ can be reduced to an unknown symmetric form, $\langle\mathrm{S}\Psi\rfloor\Psi\mathrm{R}\rangle$, isomorphic to that of ϵ, which can be seen by inspection of (3.6) to be a calculable form independent of the choice of diffraction angle [*cf.* equation (11.12) in *Goniometry*]:

$$\begin{aligned}\rho &= \epsilon\cos\psi + \eta\sin\psi\\ &= \langle\mathrm{S}\Psi\rfloor\Psi\mathrm{X}\rangle\cos\psi + \langle\mathrm{S}\Psi\lceil\Psi\mathrm{X}\rangle\sin\psi\\ &= \langle\mathrm{S}\dot{\vec{\Psi}}\Psi\rfloor\Psi\mathrm{X}\rangle = \langle\mathrm{S}\Psi\rfloor\Psi\dot{\vec{\Psi}}\mathrm{X}\rangle = \langle\mathrm{S}\Psi\rfloor\Psi\mathrm{R}\rangle\\ &= \frac{\langle\mathrm{XX}\rangle}{2} - \langle\mathrm{S}\Psi|\Psi\mathrm{X}\rangle.\end{aligned} \tag{6.6}$$

Indeed, it is this right-most calculable form that is used in practical calculations. Similarly, by direct expansion, y can be reduced to an unknown skew-symmetric form, $\langle\mathrm{S}\Psi\lceil\Psi\mathrm{R}\rangle$, isomorphic to that of η, which can be seen from the necessary relation $y^2 + \rho^2 = \eta^2 + \epsilon^2$ ($\equiv \xi^2$) deduced from (6.5) to be another form calculable without knowl-

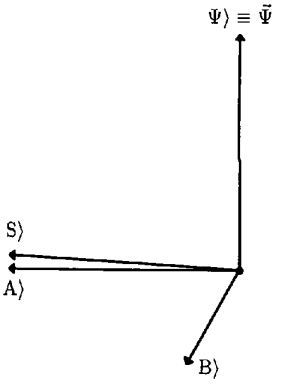

Fig. 7. The covectors used to analyse diffraction-condition geometry are drawn here for convenience in conjugate vector representation. The salient features are that $\langle\mathrm{A}$ is a linear combination of $\langle\Psi$ and $\langle\mathrm{S}$ orthogonal to $\langle\Psi$ and that $\langle\mathrm{B}$ is orthogonal to the other three.

* Notwithstanding this, there is a risk when running a FAST system with a software package designed for other machines that a thinly disguised operation equivalent to this will, in fact, be performed, with a deleterious effect, especially on determinations of the unit cell and also, particularly when profile analysis is used, on the measured intensities. Regrettably, there is a tendency for any problems to be blamed on the detector (which performs far better than is commonly realized) rather than on the mismatched operation of inappropriate software.

† Some readers have objected that y would have been better as a Greek letter in the present context, whilst acknowledging the utility of maintaining consistency with Wonacott's notation. The author would have preferred to have used a lower-case upsilon, but this is never used in mathematical formulae for obvious reasons. Perhaps an acceptable resolution would be to call the symbol upsilon anyway, though it be transliterated of necessity into the Roman alphabet.

edge of the diffraction angle [*cf.* equation (11.11) in *Goniometry*]:

$$\begin{aligned} y &= \eta\cos\psi - \epsilon\sin\psi \\ &= \langle S\Psi\rfloor\Psi X\rangle\cos\psi - \langle S\Psi\lfloor\Psi X\rangle\sin\psi \\ &= \langle S\nabla_\psi\dot{\boldsymbol{\Psi}}X\rangle = \langle S\nabla_\psi R\rangle = \langle S\Psi\rfloor\Psi R\rangle \\ &= \pm\sqrt{\eta^2+\epsilon^2-\rho^2}. \end{aligned} \tag{6.7}$$

However, y clearly does depend on the twofold choice of diffracting position. Indeed, it is the choice of sign here that defines which diffracting position we are considering, since this calculable form is the one actually used in practical calculations. Then the rotationally invariant ζ and the two (now calculated) forms for ρ and y can be used to give directly the position of the reciprocal-lattice vector in its diffracting position:

$$R\rangle = \begin{pmatrix}\langle A\\ \langle B\\ \langle\Psi\end{pmatrix}^{-1}\begin{pmatrix}\rho\\ y\\ \zeta\end{pmatrix}. \tag{6.8}$$

It will be noted that although ψ and trigonometric functions appear in this derivation, they do not appear in the computations yielding the final result. The only expensive calculation is that of the square root in (6.7).

The matrix inversion in (6.8) is usually just a formality, because the matrix being inverted is normally constant. Furthermore, in high-speed programs, such as the *GENREF* algorithm [which remains the fastest known method for prediction in the rotation method (Thomas, 1981, 1982*a*,*b*, 1985)], the choice of axes is such that the matrix is not only diagonal, and hence trivially invertible, but is also isotropic, so that it can appear as a simple scalar multiplier. If, further, (2.4) is imposed, this scalar becomes the unit multiplier and vanishes completely from computer code.

7. The generalized Lorentz factor

The Lorentz factor proper is a dimensionless quantity (see Buerger, 1960) usually defined in terms of the Bragg angle, θ, which, however, finds no application in the theory of area diffractometry. Milch & Minor (1974) gave a simpler vectorial formula having unspecified dimensions of area or possibly of volume and agreeing with Buerger's formula only when dimensionless reciprocal-lattice units are used. Many other formulae are also used, frequently mixing what are intrinsically differently dimensioned quantities, crudely defining them as dimensionless from the outset [*e.g.* Lipson's (1972*b*) formula: $L^{-1} = (\sin^2 2\theta - \zeta^2)^{1/2}$]. The use of radicals and trigonometric functions is no longer considered to be desirable and can fortunately be avoided. The newer virtualized vectorial formulae also offer considerable improvements in the efficiency with which variable experimental parameters may be refined. Here we follow the style of the basically vectorial formula of Milch & Minor, and the manner of Dr Robert Diamond (unpublished work quoted in Thomas, 1982*a*), but allowing both signs. The preferred definition is that of the signed inverse Lorentz factor given in *Goniometry* as equation (11.11) (except the change of axis to $\vec{\Phi}$):

$$L^{-1} \equiv \Upsilon = \langle S\nabla_\phi R\rangle = \langle S\Phi\rfloor\Phi R\rangle \equiv \langle R\Phi\lfloor\Phi S\rangle. \tag{7.1}$$

This is dimensioned as reciprocal area and is linear in both vector and covector arguments. For practical computations, this equation expands into

$$\Upsilon \sim (S_x \quad S_y \quad S_z)\begin{pmatrix}0 & -\Phi_z & \Phi_y\\ \Phi_z & 0 & -\Phi_x\\ -\Phi_y & \Phi_x & 0\end{pmatrix}\begin{pmatrix}R_x\\ R_y\\ R_z\end{pmatrix};$$
$$\frac{\vec{\Phi}}{\|\vec{\Phi}\|} \sim \begin{pmatrix}\Phi_x\\ \Phi_y\\ \Phi_z\end{pmatrix}. \tag{7.2}$$

We can define the conventional signed dimensionless form as $\widehat{L}^{-1} = \langle S\widehat{\Phi\rfloor\Phi}R\rangle$ where the hat implies (as usual) that unity is in some way implicated in the formula. In this case, it implies that the normalization $\langle SS\rangle = 1$ of (2.4) has been imposed. Agreement with, say, Buerger's formula is then achieved by always taking the sign as positive, but no advantage accrues from this extra (and limiting) complication. The reciprocal-lattice point must be in its diffracting position, $R\rangle = \dot{\boldsymbol{\Psi}}X\rangle$, in this formula, but this need not involve any extra computation, since this quantity appears naturally in the calculation of the diffraction geometry given in §6. A definitive definition of the Lorentz factor seems to be lacking in the literature, but (7.1) satisfies the consensus that it is inversely proportional to the rate at which a point $R\rangle$ in the reciprocal lattice penetrates the Ewald sphere with respect to changes in ϕ, described here by the form $\nabla_\phi R\rangle$. This reduces to the calculable form $\Phi\rfloor\Phi R\rangle$ using the rotationally skew-symmetric operator defined in *Goniometry*. The bilinear form, Υ, is analytically superior to the conventional Lorentz factor (which has unattractive properties near to the plane containing both the incident X-ray beam and the instantaneous rotation axis) on account of being always well behaved.

The first derivatives of the Lorentz factor are useful for establishing the dependence of collected data and other formulae on variations or uncertainties in the controlling experimental parameters, most notably $S\rangle$; then $R\rangle$, but $\vec{\Psi}$ much less so. It helps to define first the simpler derivatives of the signed dimensioned factor, Υ. The derivatives with respect to $S\rangle$ and $R\rangle$ are covector-like in reciprocal space, and those with respect to $\langle S$ and $\langle R$ are consequently vector-like in reciprocal space:

$$\nabla_{S\rangle}\Upsilon = \langle R\Phi\lfloor\Phi \iff \nabla_{\langle S}\Upsilon = \Phi\rfloor\Phi R\rangle, \tag{7.3}$$

$$\nabla_{R\rangle}\Upsilon = \langle S\Phi\rfloor\Phi \iff \nabla_{\langle R}\Upsilon = \Phi\lfloor\Phi S\rangle. \tag{7.4}$$

The two most important Jacobians of L then follow directly and are

$$\nabla_{S\rangle}L = -L^2\nabla_{S\rangle}\Upsilon = \frac{\langle R\Phi\rfloor\Phi}{\langle S\Phi\rfloor\Phi R\rangle^2} = \frac{\langle R\Phi\rfloor\Phi}{\Upsilon^2} \tag{7.5}$$

and

$$\nabla_{\mathrm{R}\rangle} L = -L^2 \nabla_{\mathrm{R}\rangle} \Upsilon = \frac{\langle \mathrm{S}\Phi\rfloor\Phi}{\langle \mathrm{S}\Phi\rfloor\Phi\mathrm{R}\rangle^2} = \frac{\langle \mathrm{S}\Phi\rfloor\Phi}{\Upsilon^2}, \qquad (7.6)$$

with conjugate forms $\nabla_{\langle \mathrm{S}} L$ and $\nabla_{\langle \mathrm{R}} L$ following by direct transposition, as in (7.3) and (7.4).

The (Hessian) second derivatives of the Lorentz factor are also useful in data analysis routines, particularly for establishing the perturbations in the results caused by the curvature of the factor within the image of a single diffraction spot. The diagonal terms are predictably symmetric and follow directly from the Jacobian terms:

$$\nabla_{\mathrm{S}\rangle\langle \mathrm{S}} L = \frac{\Phi\rfloor\Phi\mathrm{R}\rangle\, 2\,\langle \mathrm{R}\Phi\rfloor\Phi}{\langle \mathrm{S}\Phi\rfloor\Phi\mathrm{R}\rangle^3} = \frac{\Phi\rfloor\Phi\mathrm{R}\rangle\, 2\,\langle \mathrm{R}\Phi\rfloor\Phi}{\Upsilon^3}, \qquad (7.7)$$

$$\nabla_{\mathrm{R}\rangle\langle \mathrm{R}} L = \frac{\Phi\rfloor\Phi\mathrm{S}\rangle\, 2\,\langle \mathrm{S}\Phi\rfloor\Phi}{\langle \mathrm{S}\Phi\rfloor\Phi\mathrm{R}\rangle^3} = \frac{\Phi\rfloor\Phi\mathrm{S}\rangle\, 2\,\langle \mathrm{S}\Phi\rfloor\Phi}{\Upsilon^3}. \qquad (7.8)$$

The more complicated off-diagonal cross terms are antisymmetric, being

$$\begin{aligned} \nabla_{\mathrm{S}\rangle\langle \mathrm{R}} L &= \frac{\Phi\rfloor\Phi\mathrm{S}\rangle\, 2\,\langle \mathrm{R}\Phi\rfloor\Phi}{\langle \mathrm{S}\Phi\rfloor\Phi\mathrm{R}\rangle^3} + \frac{\Phi\rfloor\Phi}{\langle \mathrm{S}\Phi\rfloor\Phi\mathrm{R}\rangle^2} \\ &= \frac{\Phi\rfloor\Phi\mathrm{S}\rangle\, 2\,\langle \mathrm{R}\Phi\rfloor\Phi}{\Upsilon^3} + \frac{\Phi\rfloor\Phi}{\Upsilon^2}, \\ \Longleftrightarrow \qquad \nabla_{\mathrm{R}\rangle\langle \mathrm{S}} L &= \frac{\Phi\rfloor\Phi\mathrm{R}\rangle\, 2\,\langle \mathrm{S}\Phi\rfloor\Phi}{\langle \mathrm{S}\Phi\rfloor\Phi\mathrm{R}\rangle^3} + \frac{\Phi\rfloor\Phi}{\langle \mathrm{S}\Phi\rfloor\Phi\mathrm{R}\rangle^2} \\ &= \frac{\Phi\rfloor\Phi\mathrm{R}\rangle\, 2\,\langle \mathrm{S}\Phi\rfloor\Phi}{\Upsilon^3} + \frac{\Phi\rfloor\Phi}{\Upsilon^2}. \end{aligned} \qquad (7.9)$$

The third and higher derivatives of the Lorentz factor do not appear to be of much utility, and are not quoted here.

The Lorentz factor also has non-trivial derivatives with respect to changes in the direction of the instantaneous rotation axis, but no area detector is currently used in a way which necessitates their use.

For completeness, the second derivatives of Υ are

$$\nabla_{\mathrm{S}\rangle\langle \mathrm{S}} \Upsilon = 0, \qquad (7.10)$$

$$\nabla_{\mathrm{R}\rangle\langle \mathrm{R}} \Upsilon = 0 \qquad (7.11)$$

and

$$\nabla_{\mathrm{S}\rangle\langle \mathrm{R}} \Upsilon = \Phi\rfloor\Phi \Longleftrightarrow \nabla_{\mathrm{R}\rangle\langle \mathrm{S}} \Upsilon = \Phi\rfloor\Phi. \qquad (7.12)$$

Higher derivatives vanish. The derivatives for y are similar and are obtained by replacement of the terms in $\vec{\Phi}$ by the corresponding ones in $\vec{\Psi}$.

8. The representation of beam divergence and dispersion in first-order approximation: I

No X-ray beam is perfect, and in practice it usually makes a significant contribution to the observed angular widths of diffraction spots (Arndt & Thomas, 1985*b*). It is simplest to consider first the model most appropriate for use with a synchrotron source, where the distribution of wave vectors is usually unimodal. If the monochromator is not in the achromatic Guinier position (Guinier & Sébilleau, 1952), there will be a correlation between the angle of each component and its mean wavelength. This need not cause any analytical inconvenience if the wave-vector distribution is modelled as a triaxial Gaussian [see Thomas, 1982*a*, §2.2.3, pp. (2.4)–(2.5)], which is equivalent to describing the variance fully. This is a good first-order approximation and we have every reason to believe that it is adequate for the task of predicting the angular widths of reflexions. A second-rank tensor quantity, **S**, with the geometrical structure of a bicovector (which means that it can act upon two vectors to produce a scalar) is used to describe the variance–covariance:

$$\mathbf{S} = \left[\overline{\mathrm{S}\rangle\langle \mathrm{S}} - \overline{\mathrm{S}}\rangle\langle\overline{\mathrm{S}}\right]. \qquad (8.1)$$

This follows the normal pattern of being the mean of the squares less the square of the mean. It is represented computationally as a real symmetric positive-definite 3×3 matrix. The standard deviation of $\mathrm{S}\rangle$ is not defined because the square root of a quantity with the geometrical structure of a bicovector is not defined. Strictly, **S** is a function of position within the beam, but to a first approximation the beam is assumed to be uniform throughout the crystal, whence **S** becomes constant except for possible temporal variations. Shifts of the incident-beam wave vector are related to shifts in the diffraction angle by the Jacobian

$$\nabla_{\mathrm{S}\rangle}\phi \equiv \frac{\partial\phi}{\partial \mathrm{S}\rangle} = \frac{-\langle \mathrm{R}}{\langle \mathrm{R}\Phi\rfloor\Phi\mathrm{S}\rangle} = \frac{-\langle \mathrm{R}}{\Upsilon}, \qquad (8.2)$$

which is derived using the implicit function theorem [as equation (12.6)] in *Goniometry*. Double application of this equation to (8.1) yields directly the formula for the variance of the diffraction angle attributable to the variance of the incident-beam wave-vector distribution:

$$\begin{aligned} \mathrm{var}(\phi) \equiv \langle(\Delta\phi)^2\rangle &= \nabla_{\mathrm{S}\rangle}\phi \left[\overline{\mathrm{S}\rangle\langle \mathrm{S}} - \overline{\mathrm{S}}\rangle\langle\overline{\mathrm{S}}\right] \nabla_{\langle \mathrm{S}}\phi \\ &= \frac{\langle \mathrm{R}\,\mathbf{S}\,\mathrm{R}\rangle}{\langle \mathrm{R}\Phi\rfloor\Phi\mathrm{S}\rangle\,\langle \mathrm{S}\Phi\rfloor\Phi\mathrm{R}\rangle} = \frac{\langle \mathrm{R}\,\mathbf{S}\,\mathrm{R}\rangle}{\Upsilon^2}. \end{aligned} \qquad (8.3)$$

The variance of the diffraction angle is a scalar, so the standard deviation can also be defined by taking the square root. If **S** is approximated as $\Delta\mathbf{1}\Delta$, (8.3) reduces to the form of equation (7.41) used by Wonacott (1977), which has ξ in the denominator instead of y (which is the same as Υ for the rotation method):*

$$\mathrm{var}(\phi) \equiv \mathrm{var}(\psi) = \frac{\langle \mathrm{R}\,\Delta\mathbf{1}\Delta\,\mathrm{R}\rangle}{y^2} = \frac{\Delta^2\|\mathbf{d}^*\|^2}{y^2} = \left(\frac{\Delta d^*}{y}\right)^2$$

$$\Rightarrow \quad \mathrm{sd}(\phi) \equiv \mathrm{sd}(\psi) = \left|\frac{\Delta d^*}{y}\right|. \qquad (8.4)$$

* Wonacott's text reads somewhat ambiguously: if it is assumed that when he is referring to the distance from the axis he means as measured in the film plane, then y is appropriate; otherwise, if he means in reciprocal space, then ξ is more appropriate.

Table 5. *Symbol table for* §8 *et seq.*

$\mathrm{c}\rangle$	a vector pointing along the backstop support
$\mathrm{C}\vert\mathrm{C}$	operator resolving its argument along a line normal to both the beam and the backstop support
d_{backstop}	the diameter of the backstop cup
d^{*2}	$\equiv \Vert\mathbf{d}^*\Vert^2 = \langle\mathrm{RR}\rangle = \langle\mathrm{XX}\rangle$
$\hat{\delta}_i^j$	the Kronecker δ (1 if $i = j$, 0 otherwise)
Δ	a small number used by Wonacott (1977) for reflecting ranges
$\vec{\mathrm{E}}$	the direction of electric polarization, with right- and left-acting forms $\vert\mathrm{E}$ and $\mathrm{E}\vert$
$\epsilon^i\rangle$	a reciprocal-space vector denoting the ith component of the X-ray doublet
θ	the Bragg angle
$\mathtt{I}$	one of the axes in the pixel grid, either $\mathtt{Y}$ or $\mathtt{Z}$
$\vert\ell\vert$	an additive term to accommodate the extra spreading from the point-spread function of the detector
$\breve{\mu}$	a small-angle vector describing a mosaic misorientation
$\acute{\mu}, \grave{\mu}$	a rotation operator describing mosaic misorientation, and its inverse
$\mathbf{M}$	the mosaicity distribution tensor
p	the conventional polarization factor
P	a point within the pixel grid, $\left(P_{\mathrm{Y}}, P_{\mathrm{Z}}\right)$ [distinct from the calculated position, Q'''']
ϖ	the power in a beam
$\mathbf{\Pi}$	the beam polarization tensor
Q''''	the (distorted) position of a spot within the pixel grid, $\left(Q''''_{\mathrm{Y}}, Q''''_{\mathrm{Z}}\right) \equiv \mathrm{P}$
$\lceil\mathrm{S}\rfloor$, $\lfloor\mathrm{S}\rfloor$	the skew-symmetric operator for which $\lceil\mathrm{S}\rfloor\mathrm{R}\rangle = \mathrm{S}\rangle\wedge\mathrm{R}\rangle, \forall\ \mathrm{R}\rangle$, and its conjugate
$\mathrm{S}\lfloor\mathrm{S}$	an operator which projects its argument onto the plane normal to the incident beam
$\mathbf{S}$	the beam wave-vector distribution tensor
s	a parameter used to describe indirectly the apparent thickness of a backstop support
III	(Shah) a second-rank (bicovector-like) tensor form describing angular diffraction widths
t_{backstop}	the crystal-to-backstop distance
$t_{\mathrm{X-D}}$	the crystal-to-detector distance
$t_{\mathrm{X-S}}$	the crystal-to-apparent-source distance
$\mathrm{T}\lfloor\mathrm{T}$	an operator which projects its argument onto the plane normal to the scattered beam
V_I	the size of the crystal in the direction of the detector-plane axis, I
w_I	the width of a window in the direction of the detector-plane axis, I
$\Xi\lfloor\Xi$	an operator projecting its argument onto the plane of the beam and of the beamstop support

Wonacott's formula was designed to accommodate both isotropic mosaicity and isotropic beam divergence in the single symbol Δ, though as will become apparent in the next two sections, anisotropic distributions lead to a different law of combination.

Table 5 gives a list of symbols for this and the following sections.

9. The representation of beam divergence and dispersion in first-order approximation: II

A conventional laboratory source using an X-ray tube differs from a synchrotron source in that the wavelength distribution is bimodal. Each component of the doublet also has a small wavelength spread which need not be ignored even though it makes but a small contribution to the overall width because it can easily be included with no increase in the analytic complexity, providing that the same description as used in the last section is maintained.

The doublet splitting itself is most naturally modelled by offsetting each of the centroids of the two assumed Gaussian distributions by a small vector, $\epsilon^i\rangle$, aligned with the mean direction of the incident beam, and bound to the centroid of the complete distribution. It is less appropriate to use a standard deviation to describe the diffracting width in this case because of the asymmetry, so we use the notations $\Delta_1\phi$ and $\Delta_2\phi$ to denote the shifts in the two directions. More precisely, $\Delta_1\phi$ is used to denote the angular deviation from the mean diffracting position that makes the diffraction plane tangential to the ellipsoid describing the α_1 component of the doublet, and similarly for $\Delta_2\phi$ and the α_2 component:

$$\Delta_i\phi = \nabla_{\mathrm{S}\rangle}\phi\,\epsilon^i\rangle = \frac{-\langle\mathrm{R}\,\epsilon^i\rangle}{\langle\mathrm{R}\Phi\rfloor\Phi\mathrm{S}\rangle} = \frac{-\langle\mathrm{R}\,\epsilon^i\rangle}{\Upsilon}, \qquad (9.1)$$

where i is either 1 or 2, denoting the α_1 or the α_2 component of the doublet respectively. This model is thus an extension of that given by Thomas [1982*a*, §2.2.4, pp. (2.5)–(2.6)], where the asymmetry of the doublet and the differing dispersions of the two components were ignored.

The two components of the doublet do not have the same intensity, which means that the centroid of the distribution is not symmetrically disposed; this can be modelled adequately by adjusting the two vectors ϵ^i so that ϵ^2 is twice as long as ϵ^1:

$$\epsilon^2\rangle = -2\epsilon^1\rangle. \qquad (9.2)$$

With a simply collimated beam or one with a well adjusted monochromator, the vectors ϵ^i will be accurately parallel to $\mathrm{S}\rangle$ and can be represented computationally in reciprocal space by the two columns:

$$\epsilon^i\rangle \sim \begin{pmatrix} \epsilon^i_x \\ \epsilon^i_y \\ \epsilon^i_z \end{pmatrix}. \tag{9.3}$$

10. The representation of crystal mosaicity in first-order approximation

Mosaicity in crystals of biological macromolecules is still not generally understood particularly well. Careful observations with area-detector diffractometers show quite conclusively that some crystals, particularly native ones, are very well aligned at the microscopic level, but may exhibit long-range orientational disturbances so that the Bragg planes appear wavy on the macroscopic scale (Arndt & Thomas, 1985*b*). It is also clear that many crystallographers are led falsely to interpret the effects of poor incident-beam collimation as mosaicity (Arndt & Thomas, 1985*b*). This is understandable when using film or crude diffractometer methods of data collection, but an analysis of the full three-dimensional profiles of diffraction spots enables the two sources of broadening to be discriminated separately (Thomas, 1992*a*). However, there is also a considerable amount of evidence that other crystals, particularly heavy-atom derivatives, do display marked disordering on a microscopic scale; and, indeed, some crystals have a very short lifetime after soaking, presumably succumbing to the reduction in their stability, and disordering progressively.

Many crystals of biological macromolecules display a marked anisotropy of mosaicity and this causes a large variation in the diffracting widths of reflexions. This must be calculated properly, particularly when using dynamic windowing methods of data collection (Thomas, 1982*a*,*b*, 1985, 1986*a*,*d*, 1987; Arndt & Thomas, 1985*a*).

We can represent mosaicity as a probability density distribution expressed firstly as a function of all possible rotations and secondly also as a function of position within the crystal. An accurate and full description is therefore very complicated and leads us into the realms of profile analysis, which will be dealt with in a later paper (Thomas, 1992*b*). Mosaicity is in any case much more complicated than beam structure, and to first-order approximation we take the crystal to be so small and sufficiently homogeneous that we can neglect variations in its mosaic structure throughout its bulk, though this latter functionality will also be dealt with properly in a later paper.

For most purposes, a first-order description based on the normal or Gaussian distribution is the most useful and the mosaic misorientations, $\acute{M}$, can be modelled by means of small-angle vectors, *e.g.* $\breve{\mu}$ [see *Goniometry*, equation (9.2)]. By direct analogy with the description of the beam, the variance–covariance matrix in the small-angle vector space is denoted by a second-rank tensor, **M**. This must rotate with the crystal, so we transform it into the laboratory frame in the normal way, by double application of the rotation operator, $\dot{\mathbf{\Psi}}$, which describes the crystal rotation, as in $\mathrm{R}\rangle = \dot{\mathbf{\Psi}}\mathrm{X}\rangle$, for example, to give the form

$$\left[\overline{\breve{\mu}\rangle\langle\breve{\mu}} - \overline{\breve{\mu}}\rangle\langle\overline{\breve{\mu}}\right] = \dot{\mathbf{\Psi}}\mathbf{M}\grave{\mathbf{\Psi}}. \tag{10.1}$$

This is represented computationally by a real symmetric positive-definite 3×3 matrix. Ordinarily, we would apply the mosaic misorientation operator, $\acute{M}$, to the reciprocal-lattice vector, $\mathrm{R}\rangle$, but here it is better to apply its inverse, $\grave{M}$, to the negated representation of the incident-beam wave vector, $\mathrm{S}\rangle$, so that the contribution to the diffracting width of a spot caused by mosaicity can be combined with that caused by the imperfections of the beam. Writing $\mathrm{S}\rangle = \grave{M}\mathrm{S}_0\rangle$, the derivative of $\mathrm{S}\rangle$ with respect to the small-angle vector, $\breve{\mu}\rangle$ (defining $\acute{M}$ and $\grave{M}$) reduces to the very convenient skew-symmetric deponent form

$$\nabla_{\breve{\mu}\rangle}\mathrm{S}\rangle = \lceil\mathrm{S}\rfloor \sim \begin{pmatrix} 0 & -S_z & S_y \\ S_z & 0 & -S_x \\ -S_y & S_x & 0 \end{pmatrix}$$

$$\Longleftrightarrow \quad \nabla_{\langle\breve{\mu}}\langle\mathrm{S} = \lfloor\mathrm{S}\rceil \sim \begin{pmatrix} 0 & S_z & -S_y \\ -S_z & 0 & S_x \\ S_y & -S_x & 0 \end{pmatrix}, \tag{10.2}$$

whose action is familiar enough: it is equivalent to taking a vector cross product with $\mathrm{S}\rangle$. Although it has not been introduced before, the symbol $\lceil\cdot\rfloor$ is not really a new notation, but just a consistent development of that already defined for rotations in *Goniometry*. Its justification is as follows: a right rotation is represented by the combined presence of the two putative half-operators $\lceil$ and $\rfloor$, and the operator is linear with respect to the named quantity, so its name must appear just once; thus $\lceil\cdot\rfloor$ is an obvious and consistent choice. As a reminder, the derivation of the rotational operator $\cdot\lfloor\cdot$ included the idea that its invariance under changes of metric could be asserted by including the named quantity twice, once in a covariant and once in a cancelling contravariant representation. Like $\cdot\lfloor\cdot$, $\lceil\cdot\rfloor$ is inverted correctly by a left to right flip on the page, becoming $\lfloor\cdot\rceil$; in both cases this is seen in computational representations to be equivalent to a change of sign. By application of the derivative in (10.2) twice to (10.1), as is usual when transforming a symmetric second-rank tensor, $\dot{\mathbf{\Psi}}\mathbf{M}\grave{\mathbf{\Psi}}$ is transformed from small-angle vector space to wave-vector space. This can be written as

$$\nabla_{\breve{\mu}\rangle}\mathrm{S}\rangle \left[\overline{\breve{\mu}\rangle\langle\breve{\mu}} - \overline{\breve{\mu}}\rangle\langle\overline{\breve{\mu}}\right] \nabla_{\langle\breve{\mu}}\langle\mathrm{S} \quad = \quad \lceil\mathrm{S}\rfloor\dot{\mathbf{\Psi}}\mathbf{M}\grave{\mathbf{\Psi}}\lceil\mathrm{S}\rfloor, \tag{10.3}$$

and it therefore follows, multiplying twice by $\nabla_{\mathrm{S}\rangle}\phi$ [by

direct analogy with (8.3)], that the variance of the diffraction angle attributable to mosaicity is

$$\mathrm{var}(\phi) \equiv \langle(\Delta\phi)^2\rangle = \frac{\langle \mathrm{R}\,[\mathrm{S}]\dot{\boldsymbol{\Psi}}\mathbf{M}\dot{\boldsymbol{\Psi}}[\mathrm{S}]\,\mathrm{R}\rangle}{\langle \mathrm{R}\Phi[\Phi\mathrm{S}\rangle\,\langle \mathrm{S}\Phi]\Phi\mathrm{R}\rangle} = \frac{\langle \mathrm{R}\,[\mathrm{S}]\dot{\boldsymbol{\Psi}}\mathbf{M}\dot{\boldsymbol{\Psi}}[\mathrm{S}]\,\mathrm{R}\rangle}{\Upsilon^2}. \quad (10.4)$$

Again, the variance of the diffraction angle as defined here is a scalar, so the standard deviation can also be defined. A slight expansion of the fuller term in (10.4) shows reassuringly that $\dot{\boldsymbol{\Psi}}$ serves only to transform quantities from the moving reference frame back to the stationary one as the crystal rotates, using the normal rule of one occurrence for a first-rank tensor (X⟩) and two for a second-rank (**M**):

$$\frac{\langle \mathrm{X}\dot{\boldsymbol{\Psi}}\,[\mathrm{S}]\,\dot{\boldsymbol{\Psi}}\mathbf{M}\dot{\boldsymbol{\Psi}}\,[\mathrm{S}]\,\dot{\boldsymbol{\Psi}}\mathrm{X}\rangle}{\langle \mathrm{X}\dot{\boldsymbol{\Psi}}\,\Phi[\Phi\mathrm{S}\rangle\,\langle \mathrm{S}\Phi]\Phi\,\dot{\boldsymbol{\Psi}}\mathrm{X}\rangle}.$$

S⟩ and $\vec{\Phi}$ are fixed relative to the laboratory, whilst X⟩ and **M** are tied to the rotating crystal. Thus defined, all of the groups displayed above are referred to the laboratory frame.

11. Combining the contributions to the angular width of diffraction spots

The first-order (Gaussian) approximations to the spreading caused by the mosaicity and by the spread of each spectral component of the beam add linearly in their representation as variance–covariance tensors; indeed, it is precisely for this reason that they were both expressed in the same space as R⟩, so that

$$\mathrm{var}(\phi) \equiv \langle(\Delta\phi)^2\rangle = \frac{\langle \mathrm{R}\,\text{Ш}\,\mathrm{R}\rangle}{\langle \mathrm{R}\Phi[\Phi\mathrm{S}\rangle\,\langle \mathrm{S}\Phi]\Phi\mathrm{R}\rangle} = \frac{\langle \mathrm{R}\,\text{Ш}\,\mathrm{R}\rangle}{\Upsilon^2}, \quad (11.1)$$

where

$$\text{Ш} = \mathbf{S} + [\mathrm{S}]\dot{\boldsymbol{\Psi}}\mathbf{M}\dot{\boldsymbol{\Psi}}[\mathrm{S}]. \quad (11.2)$$

The physical quantity represented by the symbol 'Ш' has always been called 'digamma' in computer programs regardless of the names of the various algebraic symbols that have been used for it. In fact, the formula given here turns out to be an incomplete expression of an extremely important quantity, also written 'Ш', which dominates the analysis of the three-dimensional profiles of diffraction spots, but this will be discussed in the later papers (Thomas, 1992*a*,*b*). The missing term does not affect the equations of this paper. There is no doubt that **M** and **S** are genuine tensor properties but the precise physical status of Ш is slightly unclear, because it is an obviously contrived quantity which varies with the relative orientation of the crystal and the diffractometer: nonetheless, it is usually thought of as an 'honorary' second-rank tensor, on the basis of its transformational properties under rotation and the characteristic way in which it enters (11.1).

Thus the square root of (11.1),

$$\mathrm{sd}(\phi) = \frac{\sqrt{\langle \mathrm{R}\,\text{Ш}\,\mathrm{R}\rangle}}{\langle \mathrm{S}\Phi]\Phi\mathrm{R}\rangle} = \frac{\sqrt{\langle \mathrm{R}\,\text{Ш}\,\mathrm{R}\rangle}}{\Upsilon}, \quad (11.3)$$

is the simplest known equation which adequately represents all the major trends in diffraction widths displayed by small crystals with an overtly triaxial mosaicity distribution illuminated by synchrotron radiation emanating from a monochromator in a general (*i.e.* non-Guinier) position.

For a conventional source, the doublet contribution must also be included. The contributions to the angular widths of spots arising from the doublet splitting and from the dispersion and divergence in normal approximation add linearly, as can be seen from Fig. 8, so we sum the square root of (11.1) and (9.1) to give the final form for a conventional source:

$$\Delta_i\phi = \frac{-\langle \mathrm{R}\,\epsilon^i\rangle \oplus \sqrt{\langle \mathrm{R}\,\text{Ш}_i\,\mathrm{R}\rangle}}{\langle \mathrm{R}\Phi[\Phi\mathrm{S}\rangle} = \frac{-\langle \mathrm{R}\,\epsilon^i\rangle \oplus \sqrt{\langle \mathrm{R}\,\text{Ш}_i\,\mathrm{R}\rangle}}{\Upsilon}, \quad (11.4)$$

in which the special addition sign indicates that the sign of the second (radical) term necessarily follows the net sign of the first. The notation Ш_i allows the possibility of having the two different ellipsoidal descriptions, $\mathbf{S}_i$,

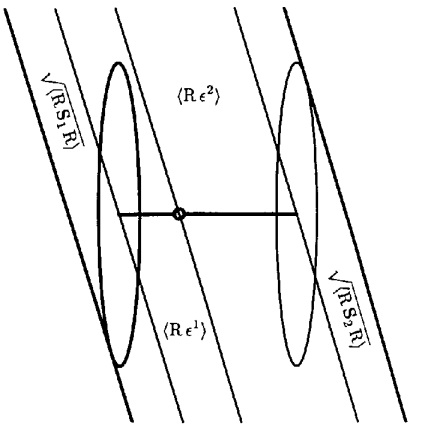

Fig. 8. A model of the doublet structure. This is a 'close-up view' of the diffraction plane sweeping through the bimodal incident X-ray wavevector distribution (*i.e.* doublet) for a conventional laboratory source. The small circle marks the centroid of the distribution, which is the position used generally for all first-order calculations of the diffraction geometry. Each ellipsoidal surface represents a suitably low contour in a Gaussian approximation to each component of the doublet. The diagram shows why the contribution from the doublet splitting and the contributions from singlet dispersion and beam divergence are summed linearly. With simple collimating optics the ellipsoids would normally be expected to be principally aligned as shown (*i.e.* one principal axis of each ellipsoid is parallel to the mean beam direction). With a monochromator not in the Guinier position, as can occur typically on a synchrotron source (where there is also no doublet splitting), the ellipsoidal orientation will not be in any way special. This figure is adapted from Fig. 3 in Thomas (1982*a*).

one for each component of the alpha doublet, by obvious extension of (11.2). These equations occur in §§2.2.3–5 of Thomas (1982*a*) in an older style of notation, and are known to fit experimental data as adjudged by the performance of the data-reduction routines run at Cambridge and elsewhere (Renetseder, Dijkstra, Kalk, Verpoorte & Drenth, 1986). This final model is thus an extension of that given by Thomas [1982*a*, §2.2.5, pp. (2.6)–(2.7)], which has been used for many years in the well tested *GENREF* algorithm for predicting diffraction spots dynamically at the highest possible speed. It is thought to be adequate for all foreseeable applications. The two distributions $\mathbf{S}_1$ and $\mathbf{S}_2$ should differ slightly because the more energetic component of the doublet has a slightly larger spread of energy, but the difference is so small that we can continue safely to ignore it.

$\mathbb{III}$ need not be calculated for each diffraction spot if they are handled in groups of similar diffraction angle, ψ, and in practice we normally compute it about once every degree of crystal rotation during continuous dynamic data collection, or once per frame or per film using the camera-type of rotation method.

12. An accurate tensorial description of beam polarization

The polarization intensity structure of an X-ray beam can be represented by a deponent second-rank tensor, say $\mathbf{\Pi}$, with the computational structure of a real-symmetric positive 3×3 matrix (Thomas, 1986*b*):

$$\mathbf{\Pi} \sim \begin{pmatrix} \Pi_x^x & \Pi_x^y & \Pi_x^z \\ \Pi_y^x & \Pi_y^y & \Pi_y^z \\ \Pi_z^x & \Pi_z^y & \Pi_z^z \end{pmatrix}. \tag{12.1}$$

This definition relies on the relative power radiated into a beam with its electric polarization along $\vec{\mathrm{E}}$ being proportional to

$$\varpi = |\mathrm{E}\mathbf{\Pi}\mathrm{E}|, \tag{12.2}$$

and on the existence of a satisfactory rule for transforming the tensor when a beam is reflected. |E and E| here satisfy |EE| = 1 and take the rôles of unit vectors or pointers. The purpose of setting |EE| = 1 is not that the value 1 has any particular significance but rather that lacking any relevance the quantities are thus represented in the most self-effacing way. The real significance of a unit vector, in any case, is not so much that its length is 1 but that no meaning whatever attaches to its length, which is why the term 'pointer' is preferred and why $\vec{\mathrm{E}}$ is defined so simply as just a 'direction'.

Geometrically, at least locally, a beam which has been rotated cannot be distinguished from one which has been reflected, so by analogy with the normal rotational transformation law for a second-rank tensor, the transformation law for this tensor during a single reflexion can be defined as

$$\mathbf{\Pi}' = \mathrm{T}\rfloor\mathrm{T}\,\mathbf{\Pi}\,\mathrm{T}\rfloor\mathrm{T}, \tag{12.3}$$

where the projective operator,

$$\mathrm{T}\rfloor\mathrm{T} = \left[\mathbf{1} - \frac{\mathrm{T}\rangle\langle\mathrm{T}}{\langle\mathrm{TT}\rangle}\right] \sim \begin{pmatrix} 1-l^2 & -ml & -nl \\ -lm & 1-m^2 & -nm \\ -ln & -mn & 1-n^2 \end{pmatrix};$$

$$\begin{pmatrix} l \\ m \\ n \end{pmatrix} = \frac{\cdot\,\mathrm{T}\rangle}{\|\mathrm{T}\rangle\|}, \tag{12.4}$$

is completely equivalent in function and form to the rotationally symmetric operator, $\cdot\rfloor\cdot$.* The possibly unexpected absence of a specific representation of the direction of motion of the incident photon in this equation is not an oversight, but a useful simplification; it is possible because $\mathbf{\Pi}$ must necessarily have a null eigenvector along that direction, so the information is included automatically. Indeed, it is this which explains the use of T⌋T above: it is uniquely an idempotent operator which has a null eigenvector along the direction of motion of the scattered beam and of itself induces no rotation. [Consider (3.5), stripping out the $\cdot|\cdot$ term which now corresponds to the direction of motion of the photon, and also setting the angle of rotation to zero: the $\cdot\lfloor\cdot$ term vanishes, leaving only the $\cdot\rfloor\cdot$ term.]

From this it follows that the value of $\mathbf{\Pi}$ for an unpolarized incident beam (along S⟩) is

$$\mathbf{\Pi} = \mathrm{S}\rfloor\mathrm{S}\mathbf{1}\mathrm{S}\rfloor\mathrm{S} = \mathrm{S}\rfloor\mathrm{S} \tag{12.5}$$

which is derived by modelling the source as a randomly vibrating charge, so that it radiates unpolarized radiation isotropically in all directions, with a corresponding isotropic polarization tensor represented adequately by $\mathbf{1}$. The power, ϖ, in a direct or in a scattered beam is then given by the correspondence product of $\mathbf{\Pi}$ or of $\mathbf{\Pi}'$ with the identity operator. The correspondence product is the same as any well defined inner product, so its action can be demonstrated easily in matrix notation. The formula is then seen to correspond to taking the trace of the square symmetric matrix representing $\mathbf{\Pi}$ or $\mathbf{\Pi}'$:

$$\varpi = \mathbf{1} \blacksquare \mathbf{\Pi} \sim \hat{\delta}_i^j \Pi_i^j \tag{12.6}$$

or

$$\varpi' = \mathbf{1} \blacksquare \mathbf{\Pi}' \sim \hat{\delta}_i^j \Pi_i'^j. \tag{12.6'}$$

It is not difficult to show that this is identical to

$$\varpi' = \mathrm{T}\rfloor\mathrm{T} \blacksquare \mathbf{\Pi}, \tag{12.7}$$

which involves fewer numerical computations overall, since $\mathbf{\Pi}'$ need not be evaluated.

The conventional polarization factor, p [*inter alia*: Buerger, 1960, ch. 3, equation (14); Lipson, 1972*a*], is given by the ratio of ϖ' to ϖ:

$$p = \frac{\varpi'}{\varpi} = \frac{\mathrm{T}\rfloor\mathrm{T} \blacksquare \mathbf{\Pi}}{\mathbf{1} \blacksquare \mathbf{\Pi}}. \tag{12.8}$$

* See equations (3.5) and (5.8) in *Goniometry*. The quadruple occurrence of the argument referred to in § 3 of *Goniometry* is displayed clearly here in equation (12.4).

Computational efficiency can be much improved by defining a normalized polarization tensor,

$$\hat{\mathbf{\Pi}} = \frac{\mathbf{\Pi}}{\mathbf{1} \blacksquare \mathbf{\Pi}}, \tag{12.9}$$

whence

$$p = \mathrm{T}\rfloor\mathrm{T} \blacksquare \hat{\mathbf{\Pi}}. \tag{12.10}$$

It will be noticed that, yet again, it has been possible to avoid trigonometric functions in a formula which has hitherto invariably used them.

The computational representation of this calculation can be demonstrated by considering, for example, how it appears using dimensionless reciprocal-lattice units for a perfectly aligned four-circle diffractometer, when it reduces to the well known conventional formula. First the incident beam is specified as pointing into the X-ray source along the laboratory x axis:

$$\mathrm{S}\rangle \sim \begin{pmatrix} 1 \\ 0 \\ 0 \end{pmatrix}, \tag{12.11}$$

as is conventional for a CAD-4 using the manufacturer's specification of the laboratory frame. For a simple collimator, it is then a safe assumption that half of the total power in the beam is polarized along y and half along z:

$$\hat{\mathbf{\Pi}} \sim \begin{pmatrix} 0 & 0 & 0 \\ 0 & \frac{1}{2} & 0 \\ 0 & 0 & \frac{1}{2} \end{pmatrix}. \tag{12.12}$$

On a conventional four-circle diffractometer using equatorial geometry, the scattered beam would be represented in terms of the Bragg angle, θ, which translates into the vectorial component form as

$$\mathrm{T}\rangle \sim \begin{pmatrix} -\cos 2\theta \\ \pm \sin 2\theta \\ 0 \end{pmatrix}, \tag{12.13}$$

though the trigonometric functions would never be evaluated with an area detector; the equation is purely illustrative. Direct expansion of the formula for $\mathrm{T}\rfloor\mathrm{T}$ yields

$$\mathrm{T}\rfloor\mathrm{T} \sim \begin{pmatrix} 1 - \cos^2 2\theta & \mp \sin 2\theta \cos 2\theta & 0 \\ \mp \cos 2\theta \sin 2\theta & 1 - \sin^2 2\theta & 0 \\ 0 & 0 & 1 \end{pmatrix}, \tag{12.14}$$

though in this particular case it might have been noted that the evaluation of the first column and of the first row was unnecessary because of the structure of $\hat{\mathbf{\Pi}}$. Equation (12.10) now gives directly

$$\begin{aligned} p = \mathrm{T}\rfloor\mathrm{T} \blacksquare \hat{\mathbf{\Pi}} &\sim \begin{pmatrix} 1 - \cos^2 2\theta & \mp \sin 2\theta \cos 2\theta & 0 \\ \mp \cos 2\theta \sin 2\theta & 1 - \sin^2 2\theta & 0 \\ 0 & 0 & 1 \end{pmatrix} \\ &\quad \blacksquare \begin{pmatrix} 0 & 0 & 0 \\ 0 & \frac{1}{2} & 0 \\ 0 & 0 & \frac{1}{2} \end{pmatrix} \\ &= 1 - \frac{\sin^2 2\theta}{2} = \frac{1 + \cos^2 2\theta}{2} \end{aligned} \tag{12.15}$$

which is identical to the conventional formula for the same geometry. Equation (12.10) is, however, more efficiently computable, lacking the cosine function.

13. Calculation of the window to cover a diffraction spot

Most methods of data collection or of data reduction require a rectangular window of pixels covering the diffraction spot to be selected for further analysis as a means of reducing the total number of data and of excluding other orders of diffraction. Although an accurate calculation of the projected shape of diffraction spots on the surface of the detector is available [and will be presented in a sequel to this paper: Thomas (1992*a*)], it is not necessary to invoke such an elaborate analysis just to determine the size of a window large enough to record a diffraction spot without clipping it. The calculation given here is that used within the software package written for the FAST system at Cambridge. In this case, an old-fashioned style of formula is still used, without the advantages of the more modern vectorial or coordinate-free styles, though computationally expensive explicit trigonometric calculations are still avoided. Some accuracy is sacrificed, but in such a way that the approximations tend to increase the size of the window. The calculation assumes both a simply collimated X-ray beam emanating from a point source and that the origin of the detector coordinates, Q = 0, is at the point on the detector nearest to the crystal so that $\mathrm{d}^{\perp} = \mathrm{d}^{O}$. The width, w_I, of a window in the direction of the detector-plane axis, I (as can be deduced directly from the diagram in Fig. 9) is

$$w_I \approx V_I \frac{\sqrt{Q_I^2 + t_{\mathrm{X-D}}{}^2}}{t_{\mathrm{X-D}}} \frac{t_{\mathrm{X-S}} + \sqrt{Q_I^2 + t_{\mathrm{X-D}}{}^2}}{t_{\mathrm{X-S}}} \tag{13.1$_I$}$$

where V_I is the extremal size of the crystal measured in the direction of the detector-plane axis, I. The first fraction accounts for the lengthening of the spot at inclined incidence and is equal to the secant of the projected angle of incidence providing that the detection surface is planar. The second fraction accounts for the relative magnification of the spot, assuming that the X-rays radiate along straight lines from a point source at a distance $t_{\mathrm{X-S}}$ from

the crystal.* The terms Q_I are defined in (5.4_I). Then, to calculate the size of the window in pixels, we use the approximate formula

$$\Delta P_{\rm I} \approx \left|\frac{\partial Q''''_{\rm I}}{\partial Q_Y} w_Y\right| + \left|\frac{\partial Q''''_{\rm I}}{\partial Q_Z} w_Z\right| + |\ell| \qquad (13.2_{\rm I})$$

which includes automatically the desired tendency to overestimate the size of the measurement window. The extra, positive, additive term, $|\ell|$, whose value is usually taken to be 2.0 px increases further the size of the measurement window, partly to allow for the major part of the spread of the image of the spot because of the point-spread function (Thomas, 1990*b*), and partly just as a safety precaution to allow a certain tolerance in the prediction of the position of the diffraction spot. Equations (13.2), being based on the Jacobian of the spatial distortions, also adjust the size of the window automatically to accommodate the increasing distension of the observed images of the spots towards the sides and corners of the detection area (see Thomas, 1989).

In fact, (13.1) can easily be made more like a fully vectorial form by some simple substitutions. Note first that $t_{\rm X-D} \equiv \|{\rm d}^{\perp}\|$ and that a similar formula would exist for $t_{\rm X-S}$ though we do not normally use a direct-space vector pointing from the crystal to the assumed point source of X-rays. The form $Q_I^2 + {t_{\rm X-D}}^2$ is then replaced with the quadratic form, $\{\Theta\, {}^{\rm x}_{I}{\rm d}\lfloor{\rm d}^{\rm x}_{I}\,\Theta\}$, where ${}^{\rm x}_{I}{\rm d}\lfloor{\rm d}^{\rm x}_{I}$ is [like the rotationally symmetric operator, $\cdot\lfloor\cdot$, in Thomas (1990*a*)] an idempotent real symmetric matrix of rank 2 having its null eigenvector along the detector Y axis if $I = Z$, or along the detector Z axis if $I = Y$. This yields

$$w_I \approx V_I \frac{\sqrt{\{\Theta\, {}^{\rm x}_{I}{\rm d}\lfloor{\rm d}^{\rm x}_{I}\,\Theta\}}}{\|{\rm d}^{\perp}\|} \frac{t_{\rm X-S} + \sqrt{\{\Theta\, {}^{\rm x}_{I}{\rm d}\lfloor{\rm d}^{\rm x}_{I}\,\Theta\}}}{t_{\rm X-S}}. \qquad (13.3_I)$$

This formula still differs from the usual 'vectorial style' in as much as it represents the extent of the crystal in direct space by a parallelogram whose plane is parallel to that of the detector, whereas two- or three-dimensional distributions are normally represented by Gaussian or elliptical forms. However, one could hardly claim that the shapes of most crystals are represented better by an ellipse than by a rectangle, and given that we invariably use rectangular windows in the pixel grid, there is no reason to adapt (13.3) any further unless the crystal is rotated about the beam during data collection.

* There is a further implicit approximation involved which is that the crystal is also V_I thick in the direction of the beam and is of circular section in the plane illustrated so that the beam does not change section on reflexion. This is considered to be generally justifiable at the level of accuracy required and also has the desired effect of increasing slightly the calculated width at the detector. Dr R. Diamond has kindly pointed out that a crystal in the form of a thin plate normal to the beam would result in the equation $w_I \approx V_I \left[1 + (Q_I^2 + {t_{\rm X-D}}^2)/(t_{\rm X-S} t_{\rm X-D})\right]$.

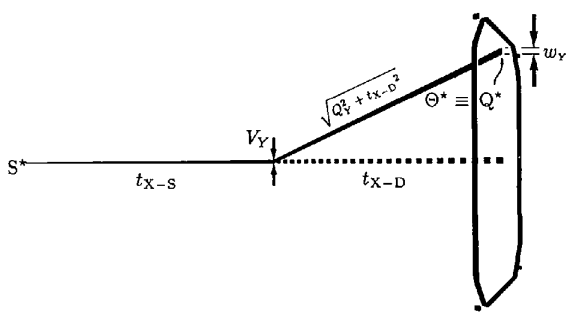

Fig. 9. The maximum possible size of a diffraction spot on the detector. This is calculated to a sufficient accuracy by tracing rays emanating from an assumed point source (typically about 220 mm from the crystal on a CAD-4) through the crystal to the detector. As noted in the footnote to the text, it is assumed that the beam does not change section passing through the crystal, which is the same as assuming that the crystal is as thick in the direction of the incident beam as it is wide in the direction marked, and is also of approximately circular section in the plane illustrated.

14. The shadow of the backstop

The first two equations of §13 survive in current code – even though the 'vectorial-style' equivalent could easily be substituted – mainly because there has been no particular pressure to increase the versatility or machine independence at that point. The emphasis is in any case rather different with calculations of the region of a diffraction pattern occluded by a backstop, because the geometries of backstops appear to be too varied to be accommodated efficiently with a single formula. It still seems to be better to adopt an *ad hoc* calculation specific to the instrument in use. There is no reason why a selection of appropriate formulae cannot be pre-programmed, so that all of the backstops normally used on a given installation can be selected at run-time through the normal parsing routine. The equations used during dynamic data collection on the FAST system at Cambridge are given here as an example. This system collects data according to a strict rule: that all measurements of diffraction spots are complete (*i.e.* there are no 'partials') and no rejections are made *for any reason* after the measurement has been made; the corollary of this is that some measurements must be prevented from occurring. In practice those measurements which could be endangered by an obstruction such as the backstop or the mask delimiting the edge of the detection area are prevented by prior cancellation, as are spots diffracting beyond a certain predefined resolution limit.

The resolution is calculated most conveniently using the traditional variable, $d^{*2} \equiv \|\mathbf{d}^*\|^2 = \langle {\rm RR}\rangle = \langle {\rm XX}\rangle$, which is already available as a by-product of the calculation of the position at which a spot will strike the detector plane, being a part of (6.6). For reasonably monochromatic incident X-rays, the shadow of the backstop cup is modelled by a lower limit on d^{*2}, calculated from the following formula:

$$d^{*2}{}_{\rm min} = \left(\frac{d_{\rm backstop} k}{t_{\rm backstop}}\right)^2, \qquad (14.1)$$

where d_{backstop} and t_{backstop} respectively are the diameter (*N.B.*! *not* radius) of the backstop and the distance from its front rim to the crystal; k is the mean wavenumber of the X-ray beam, expressed in the same units as d^{*2}. This part of the backstop-rejection calculation is likely to be common to all experimental arrangements; it has the rather safe property of rejecting all spots which might have any part clipped by the backstop cup. The second part, which relates to the strip supporting the cup, may well not be: some backstops are supported on a very thin membrane, others by a single 'edge-on' strip and, less commonly, by more than one strip or rod-like member. Equally, the supporting strip or rod may be parallel sided or may be tapered and so on. For the FAST system, the strip is modelled as a parallel-sided obstruction aligned along the detector Y axis (vertically upwards on a normal installation), and whose width is about one third of the diameter of the cup. Two new geometrical quantities are invoked: the first is an operator of rank 1 which is nilpotent in the directions of the incident beam and a line within the backstop support, say C|C; the second is also an operator of rank 1, representing a vector pointing along the same line within the backstop support, say c⟩, though it is used here in its covector form, ⟨c. Strictly, C|C must satisfy

$$\text{C|C} \blacksquare \Xi|\Xi = 0, \qquad (14.2)$$

where $\Xi|\Xi$ is an operator projecting its argument onto the plane containing both the mean line of the incident beam, S⟩, and the line, c⟩, within the backstop support. This definition forces C|C to be a representation of the normal to that plane.

A diffraction spot will then be rejected if

$$\langle \text{RC|CR} \rangle < s\, d^{*2}{}_{\min} \quad \text{and} \quad \langle \text{cR} \rangle > 0, \qquad (14.3)$$

which is illustrated in Fig. 10. The value of s, which defines the square of the ratio of the apparent thickness of the backstop support to the size of the cup is normally taken to be *ca* 0.1. These calculations tend to produce a cut-out around the backstop which is larger than the perceived shadow and might therefore be considered somewhat more cautious, which is appropriate when attempting to collect reliable data. They are also much simpler to implement, and less temperamental, than the alternative approach of trying to delimit an observed backstop shadow.

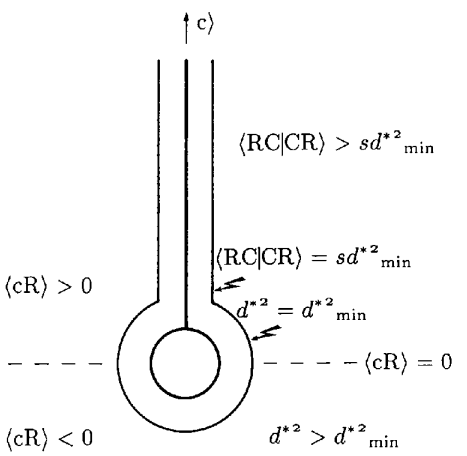

Fig. 10. Occlusion by a simple backstop. When the reliability of data is important, it is better to reject by calculation those spots which might be clipped, rather than trying to discriminate unreliably the extent of the soft-edged backstop shadow from a noisy image. The calculation for a FAST system shown here relies on three simple inequalities which cost very little extra computation.

15. Surveying a diffraction pattern for assessment and prealignment

One of the best methods of assessing a crystal on an area-detector camera or diffractometer is to align it so that a net plane of the reciprocal lattice is roughly perpendicular to the incident X-ray beam, and then to take a small-angle precession photograph. With a properly calibrated system, a relatively good estimate of the orientation of the crystal (called a 'prealignment') can then be obtained from the centroids of the spots in the image, which fall into readily distinguishable rings. The equations describing the necessary motions of the goniostat to bring a supposed plane normal into alignment with the beam and then to perform a precession motion have already been given in *Goniometry*, §§ 8–9. Here the discussion is confined to a manual method of determining the (direct-space) zone axis from the image as used on the FAST system at Cambridge, though some users prefer to use automatic indexing routines when the diffraction pattern is 'clean' enough.

We first make a reasonably short exposure and then start the assessment by positioning the cross-wire on the monitor screen over one of the observed spots. This can still be done most conveniently by hand using either a 'mouse' or the cursor keys on the controlling keyboard. The cross-wire position, P, produced this way will typically be accurate only to within a pixel or two, but this is usually accurate enough to index the spot if a rough cell matrix is already known. The computer program inverts the spatial distortions of the detector to give the approximate position of the spot on the detector faceplate or in the unit square of the spatial-distortion calculations (see Thomas, 1989, equation 6.2):

$$''''\text{P} \leftarrow \aleph^{-1}(\text{P}) \quad \text{or} \quad '''\text{P} \leftarrow \Delta^{-1} M^{-1} \Pi^{-1}(\text{P}). \qquad (15.1)$$

(See Table 6.) This yields immediately the full three-dimensional description of the scattered ray emanating from the crystal:

$$\Theta\} = (\,\text{d}^Y \quad \text{d}^Z \quad \text{d}^O\,) \begin{pmatrix} ''''P_Y \\ ''''P_Z \\ 1 \end{pmatrix}$$

$$\equiv (\,\text{d}'^Y \quad \text{d}'^Z \quad \text{d}'^O\,) \begin{pmatrix} '''P_Y \\ '''P_Z \\ 1 \end{pmatrix}. \qquad (15.2)$$

Table 6. *Symbol table for* §15

$\aleph$	(aleph) the complete imaging process of the detector (Thomas, 1989)
$\dot{\mathbf{C}}$	a constrained rotation, also used as the orientation of the centre of a precession motion
Δ	the formal name of the principal distortion transformation
$\mathbf{M}_\diamond$	an accumulated observational normal matrix
m	a scalar weighting factor for each diffraction spot
N°	the ordinal number of a ring in a diffraction pattern
$'''\mathrm{P}$	the result of pulling P back through Π, M and Δ, $= \left('''P_Y, '''P_Z\right)$
$''''\mathrm{P}$	the result of pulling P back from the pixel grid to the detection plane, as $\aleph^{-1}(\mathrm{P})$
p	a dummy argument representing P
Π	the formal name of the pixel-allocation transformation
W_c	the integrated corrected observed intensity, dimensioned as 'counts'
$w_c(\mathrm{P})$	the corrected observed intensity at P, dimensioned as 'counts per pixel area'
$\mathrm{Z}\langle$	a zone axis; the special notation insists that the dimensioning be inverse to the reciprocal-space vectors
$\mathrm{z}\rangle$	an accumulated 'observational vector'
$\iint_{\bigcirc} \mathrm{d}^2 \cdot$	a special area integral over a circular window, considered as an indivisible algebraic operation

This vector can then be rescaled to give the reciprocal-space representation of the scattered beam:

$$\mathrm{T}\rangle = \frac{\|\mathrm{S}\rangle\|}{\|\Theta\}\|}\Theta\}, \tag{15.3}$$

and hence the reciprocal-lattice vector in the diffracting position:

$$\mathrm{R}\rangle = \mathrm{T}\rangle + \mathrm{S}\rangle. \tag{15.4}$$

Using the central orientation, $\dot{\mathbf{C}}$ [see *Goniometry*, equation (8.19)], of the precession motion to represent the approximate orientation of the crystal when the spot was diffracting, an approximate datum orientation of the corresponding reciprocal-lattice vector is then given by

$$\mathrm{X}\rangle = \grave{\mathbf{C}}\mathrm{R}\rangle, \tag{15.5}$$

where $\grave{\mathbf{C}}$ is the rotation inverse to $\dot{\mathbf{C}}$. If an approximate conventional direct-space unit-cell matrix is known, the indices of the spot can be estimated as

$$\mathrm{h} \equiv (h, k, \ell) = \left[\langle \mathbf{XF} \right]. \tag{15.6}$$

The square parentheses here denote rounding to the nearest integer. This is not necessarily the nearest reciprocal-lattice point, but no errors arise until the calculated indices before rounding are so far from any lattice point (*i.e.* roughly half-way between) that the possibility of determining a correct assignment would be considered implausible. In practice, these indices are displayed on the VDU continually while the crystallographer is moving the cross-wire, and can be a very useful check on program operation. Once the crystallographer has decided to make use of a given spot, the number, N°, of the ring that it occupies is typed in. The centroid of the image of the spot is then determined accurately by integration within a soft-edged circular window using the same special Weber–Hermite integral as is used in calibration procedures (Thomas, 1989, 1990*b*) and in profile analysis. The integral over the background-corrected image, written

$$W_c = \iint_{\bigcirc} \mathrm{d}^2\mathrm{p}\; w_c(\mathrm{p}), \tag{15.7}$$

gives a good estimate of the perceived intensity of each diffraction spot, and it can be used to divide the first moment to give the error of the cross-wire position in pixels:

$$\overline{\Delta\mathrm{P}} = \frac{1}{W_c} \iint_{\bigcirc} \mathrm{d}^2\mathrm{p}\; w_c(\mathrm{p})\,(\mathrm{p} - \mathrm{P}). \tag{15.8}$$

A second-rank quantity is similarly defined from the second moment:

$$\overline{\Delta\mathrm{P} \otimes \Delta\mathrm{P}} = \frac{1}{W_c} \iint_{\bigcirc} \mathrm{d}^2\mathrm{p}\; w_c(\mathrm{p})\,(\mathrm{p} - \mathrm{P}) \otimes (\mathrm{p} - \mathrm{P}). \tag{15.9}$$

These quantities are sufficient to define a weighted inverse variance–covariance matrix,

$$W_c \left[\overline{\Delta\mathrm{P} \otimes \Delta\mathrm{P}} - \overline{\Delta\mathrm{P}} \otimes \overline{\Delta\mathrm{P}}\right]^{-1}. \tag{15.10}$$

The square root of the determinant of this 2×2 matrix is evaluated to form a scalar weight for each diffraction spot:

$$m = \sqrt{\left| W_c \left[\overline{\Delta\mathrm{P} \otimes \Delta\mathrm{P}} - \overline{\Delta\mathrm{P}} \otimes \overline{\Delta\mathrm{P}}\right]^{-1} \right|}. \tag{15.11}$$

This equation is not formally justified, but its performance is found to be adequate for practical needs. The radical form restores the result to linearity on W_c and makes it inversely proportional to a typical linear dimension of the image of the spot. If the data were three-dimensional instead, the cube root would have been taken, and so on.

Every reciprocal-lattice point, $\mathrm{X}\rangle$, when viewed down a zone axis $\mathrm{Z}\langle$, appears in a ring numbered N° given by

$$\mathrm{N}^\circ = \rangle \mathrm{ZX} \rangle. \tag{15.12}$$

The special notation for the zone axis (which is not recommended for wider use) is intended to indicate that the dimensioning of this vector must be exactly inverse to that of the reciprocal-space vector, X⟩. It is, of course, the vector in direct space and not the whole-number zone symbol $[UVW]$ that is intended. A least-squares solution obtains by minimizing the quadratic residual

$$\sum_{\mathrm{h}} \frac{(\rangle \mathrm{ZX_h}\rangle - \mathrm{N_h^\circ})\, m_\mathrm{h}\, (\langle \mathrm{X_h Z}\langle - \mathrm{N_h^\circ})}{2} \qquad (15.13)$$

summed over the set of accepted points (indexed by h). This is done by augmenting an observational vector, z⟩, and a normal matrix, $\mathrm{M}_\diamond$, with data from each new spot according to

$$\mathrm{z}\rangle = \sum_{\mathrm{h}} \mathrm{X_h}\rangle m_\mathrm{h} \mathrm{N_h^\circ} \qquad (15.14)$$

and

$$\mathrm{M}_\diamond = \sum_{\mathrm{h}} \mathrm{X_h}\rangle m_\mathrm{h} \langle \mathrm{X_h}. \qquad (15.15)$$

The diamond subscript follows the notation of Thomas (1989) in implying the presence of a hidden double dependence on a metric, in this case the one on which reciprocal-space vectors are measured. When the crystallographer is satisfied that a sufficient number of spots have been accepted, the perceived zone axis is evaluated by the usual technique of multiplying the observational vector by the inverse of the normal matrix:

$$\mathrm{Z}\langle = \mathrm{M}_\diamond^{-1}\, \mathrm{z}\rangle. \qquad (15.16)$$

In practice, we find that zone vectors determined this way are accurate to about 0.1°, which is good enough to be able to start dynamic data-collection runs (see Thomas, 1982*a*,*b*, 1985). The perceived lengths of the zone axes are usually not particularly accurate; however, considering the simplicity of the method and the approximations involved, they give no cause for complaint.

Concluding remarks

Diffraction cameras and diffractometers, whether furnished with a single counter or with an area detector, all have the same basic layout and are therefore amenable to a unified mathematical description. In this paper I have described a unifying vectorial description of all of the basic geometries necessary to enable the measurement of diffraction intensities with an area diffractometer. It has a surprisingly simple overall structure. The burden of a full component representation is avoided by using a modern coordinate-free notation. A concomitant advantage is the complete avoidance of computationally expensive and analytically inconvenient trigonometric functions. The vectorial method also simplifies the calculation of the first-derivative (Jacobian) and the second-derivative (Hessian) terms so necessary for refinement procedures and the more advanced methods of data reduction. The concept of 'misorientation angles' are avoided completely; indeed, angles in general are used only rarely when absolutely necessary. Now, instead, the Cartesian component representations of the geometric elements are refined directly. The few occasions when trigonometric calculations are unavoidable in diffractometry were formalized in *Goniometry* (Thomas, 1990*a*). Full component representations facilitate the duplication of the equations as working computer code.

It has been shown that the entire analysis of area diffractometry can be generalized using vectors and covectors manipulated with matrix algebra: the familiar isosceles triangle of the kinematic theory of diffraction can be described using a symmetric contracted notation similar to that of Dirac; the diffracting position for a given reciprocal-lattice point can be calculated for a generalized rotation method; the conventional dimensionless Lorentz factor, L (here, strictly $|\widehat{L}|$), can be redefined in favour of a simpler and more generally useful quantity, Υ; the conventional polarization factor, p, can also be re-expressed from a second-rank tensor.

The novel and previously unpublished formula for the diffracting width of a spot given here is both efficiently calculable and yet also particularly accurate, being able to accommodate quite general beam imperfections and triaxial crystal mosaicity distributions; this is accomplished using a degenerate formula for a previously unreported tensor-like quantity, III, which dominates the analysis of the full three-dimensional profiles of diffraction spots.

It would be wrong to think that it is always possible or even desirable to generalize our equations, and the calculation of the windows enclosing diffraction spots and of the shadow of the backstop have been given as counter examples. The useful manual solution to the practical problem of how to assess a diffraction pattern and to pre-align a crystal from a small-angle precession photograph shows a style typical of modern equations of diffractometry, in the sense that it combines the use of Weber–Hermite functions, correctly quantum-weighted least squares,* and some of the most powerful available geometric and notational methods.

I am grateful to Drs U. W. Arndt FRS, A. C. Bloomer, A. Guinier, S. Mason, P. A. Tucker and especially R. Diamond for help and advice whilst preparing the manuscript, and to Mary Holmes for continued help in obtaining the older references. Most of the computational work leading to this paper was supported by the Medical Research Council of Great Britain as part of the development of the Enraf–Nonius FAST system; the manuscript was completed at the European Molecular Biology Laboratory supported by an **EMBO** long-term fellowship.

* That is, each incoming photon contributes with equal weight to the final answer.

APPENDIX *A*

Some notational symmetries

It has already been noted that the notation in this and in the previous paper is so symmetric that it comprehends both the character in reciprocal space and the character in direct space simultaneously, though simple computational (*i.e.* component) forms comprehend only one of the two characters at a time. With the restricted convention that $\cdot\rangle$ is a vector in reciprocal space and that $\langle\cdot$ is a vector in direct space, a left to right flipping of an equation would be interpreted as inverting the named quantities into their mutual dual spaces: the reciprocal-space vector $\cdot\rangle$ becomes the direct-space vector $\langle\cdot$, and the direct-space vector $\langle\cdot$ becomes the reciprocal-space vector $\cdot\rangle$. It is equally valid to use the interpretation that all quantities are expressed in reciprocal space, in which case the reciprocal-space vector $\cdot\rangle$ becomes the reciprocal-space covector $\langle\cdot$ and *vice versa*; it is no less valid to use the interpretation that all quantities are expressed in direct space and the direct-space vector $\langle\cdot$ becomes the direct-space covector $\cdot\rangle$ and *vice versa*. Computationally, this left to right flipping of the equations has very much the character of transposition, much in the same way as a matrix equation can be transposed. This much was established already in *Goniometry* where, indeed, the notation was specially constructed to have these properties in order to allow the efficient solution of rotational problems. Thus, at first sight, the concise notation may already appear complete and sufficient, so long as the connection between dual spaces and Fourier transforms is not realised. At this juncture, however, a potential conundrum arises because a Fourier transform has to be applied not twice but four times to bring a system back to its starting representation; a mere double application has the effect of inverting through a centre. This immediately raises the question: 'can this notation model Fourier transformation, or is it deficient?'.

An obvious observation is that a notation capable of representing the fourfold Fourier cycle must comprehend a fourfold set of permutations on the page; two exist already, *i.e.* reading from left to right or from right to left; writing on the back of the paper, apart from being inconvenient, would give basically the same result as the left to right flip already in use if the paper were transparent enough to see it; it would seem that the only remaining choice is to write the equations upside down (or rotated 180°)!

The four ways of writing the rotationally invariant scalar form $\langle X\Psi|\Psi S\rangle$ are

$$\left\{\begin{array}{c|c}\langle S\Psi|\Psi X\rangle & \langle X\Psi|\Psi S\rangle\\ \langle S\Psi|\Psi X\rangle & \langle X\Psi|\Psi S\rangle\end{array}\right\}, \qquad (A0)$$

where the central vertical rule mediates the left to right flipping like a mirror plane, and the lower line is an upside-down representation of the upper one. In this particular case, there is no apparent difference, which is correct for a rotationally invariant scalar.

The antisymmetric scalar form, η (see Table 3), behaves differently:

$$\left\{\begin{array}{c|c}\langle S\Psi\rfloor\Psi X\rangle & \langle X\Psi\lfloor\Psi S\rangle\\ \langle S\Psi\lceil\Psi X\rangle & \langle X\Psi\rceil\Psi S\rangle\end{array}\right\}. \qquad (A1)$$

The long overlines here denote the same as a minus sign, in the conventional manner of crystallography. They are needed because the scalar forms within angle brackets on the lower line have the opposite value to those on the upper line until the minus sign is imposed. The symmetric form, ϵ, has the same property of changing sign when turned upside down:

$$\left\{\begin{array}{c|c}\langle S\Psi|\Psi X\rangle & \langle X\Psi\lfloor\Psi S\rangle\\ \langle S\Psi\lceil\Psi X\rangle & \langle X\Psi|\Psi S\rangle\end{array}\right\}, \qquad (A2)$$

as, indeed, does the alternative way of writing the antisymmetric form above, $-\eta$:

$$\left\{\begin{array}{c|c}\langle S\Psi\lfloor\Psi X\rangle & \langle X\Psi\rfloor\Psi S\rangle\\ \langle S\Psi\lceil\Psi X\rangle & \langle X\Psi|\Psi S\rangle\end{array}\right\}. \qquad (A3)$$

These are fully in agreement with any of the interpretations:

$$\left\{\begin{array}{c|c}\text{Original} & \text{Fourier}\\ \text{Original} & \text{Fourier}\end{array}\right\}$$

$$\left\{\begin{array}{c|c}\text{Normal direct space} & \text{Normal reciprocal space}\\ \text{Inverted direct space} & \text{Inverted reciprocal space}\end{array}\right\}$$

$$\left\{\begin{array}{c|c}0 & 1\\ 2 & 3\end{array}\right\}, \qquad (A4)$$

where $\overline{\text{Original}}$ means the original space inverted through a centre, and similarly for the Fourier space. The numbers $\left\{\begin{smallmatrix}0 & 1\\ 2 & 3\end{smallmatrix}\right\}$ denote the appropriate number of forward Fourier transformations starting from the original version; they are counted modulo 4. The numbering of displays (*A*0)–(*A*3) is chosen to match the four parities of the Weber–Hermite functions, which also necessarily follow the same symmetries.

Thus, it can be seen that the notation is not in any way deficient; rather, it is fully competent to unify vector/covector formulations, inversion to dual spaces and Fourier transformation. No real work is involved; it comprehends all interpretations simultaneously.

APPENDIX *B*

Restricted general inverse

The generalized inverse of singular and non-square matrices is generally credited to Moore (1920, 1935) or to Pen-

rose (1955), who was unaware of Moore's earlier work. Rao & Mitra (1971) discuss the theory and the history very clearly in the preface of their book. The article by Peters & Wilkinson (1970) may also be found useful. The use of generalized inverses here is quite restricted and can be summarized sufficiently by defining the practical computation of them.

Given a non-square matrix, say $\mathbf{F}$, define either

$$\overline{\mathbf{F}} = \left[\mathbf{F}^{\mathrm{T}}\mathbf{F}\right]^{-1}\mathbf{F}^{\mathrm{T}} \qquad (B1)$$

or

$$\overline{\mathbf{F}} = \mathbf{F}^{\mathrm{T}}\left[\mathbf{F}\mathbf{F}^{\mathrm{T}}\right]^{-1}. \qquad (B2)$$

For all of the applications here, one of the two forms above in square brackets will be a positive-definite real symmetric matrix, and hence susceptible to classical matrix inversion.

Note added in proof: The left-hand sides of equations (7.7) to (7.12), being second derivatives, should each have a superscript 2 to follow normal convention. The omission was inadvertent and should not be taken to imply an intended or desirable notational contraction.

References

ARNDT, U. W. & THOMAS, D. J. (1985*a*). Computing aspects of position-sensitive detectors. In *Crystallographic Computing* 3: *Data Collection, Structure Determination, Proteins, and Databases*, edited by G. M. SHELDRICK, C. KRÜGER & R. GODDARD, pp. 43–51. Oxford: Clarendon Press.

ARNDT, U. W. & THOMAS, D. J. (1985*b*). X-ray collimation for protein crystallography. *Aust. J. Phys.* **38**, 353–357.

ARNDT, U. W. & WONACOTT, A. J. (1977). *The Rotation Method in Crystallography*, edited by U. W. ARNDT & A. J. WONACOTT. Amsterdam: North-Holland.

BRAGG, W. L. (1913). The diffraction of short electro-magnetic waves by a crystal. *Proc. Cambridge Philos. Soc.* **17**, 43–57.

BUERGER, M. J. (1960). *Crystal-Structure Analysis*. New York: John Wiley .

BURKE, W. L. (1985). *Applied Differential Geometry*. Cambridge Univ. Press.

BUSING, W. R. & LEVY, H. A. (1967). Angle calculations for 3- and 4-circle X-ray and neutron diffractometers. *Acta Cryst.* **22**, 457–464.

DIRAC, P. A. M. (1958). *The Principles of Quantum Mechanics*, 4th ed., §§5–6, pp. 14–22. Oxford Univ. Press.

EWALD, P. P. (1913). Zur Theorie der Interferenzen der Röntgenstrahlen in Kristallen. *Phys. Z.* **14**, 465–472.

FRIEDRICH, W., KNIPPING, P. & LAUE, M. (1912). Interferenz-Erscheinungen bei Röntgenstrahlen. *Sitzungber. Math. Phys. Kl. K. Bayer. Akad. Wiss. Muenchen*, pp. 303–322.

GRIMALDI, F. M. (1665). *Physica-Mathesis de Lumine, Coloribus, et Iride, Aliisque Adnexis Libri duo ... Opus Posthumum*, edited by H. BERNIA. Bononiae: 1665. Copy in the British Library, London.

GUINIER, A. J. & SÉBILLEAU, F. (1952). Montage achromatique pour la détermination du profil de raies de diffraction des rayons X. *C. R. Acad. Sci.* **235**, 888–890.

KAHN, R. (1986). Reported in Proc. of the EEC Cooperative Workshop on Position-Sensitive Detector Software (Phase III), LURE, 12–19 November 1986, pp. 44–48. Also reported in *Computational Aspects of Protein Crystal Data Analysis*, edited by J. R. HELLIWELL, P. A. MACHIN & M. Z. PAPIZ. Proc. of the Daresbury Study Weekend, 23–24 January 1987. Report DL/SCI/R25, SERC Daresbury Laboratory, Warrington, England.

KLINGER, A. L. & KRETSINGER, R. H. (1989). *LATTICEPATCH* – an interactive graphics program to design data measurement strategies for area detectors. *J. Appl. Cryst.* **22**, 287–293.

LAUE, M. (1912). Eine quantitative Prüfung der Theorie für die Interferenz-Erscheinungen bei Röntgenstrahlen. *Sitzungber. Math. Phys. Kl. K. Bayer. Akad. Wiss. Muenchen*, pp. 363–373.

LIPSON, H. (1972*a*). In *International Tables for X-ray Crystallography*, Vol. II, §5.1 Basic definitions and formulae, p. 237, equations (2), (3) *et seq.* Birmingham: Kynoch Press. (Present distributor Kluwer Academic Publishers, Dordrecht.)

LIPSON, H. (1972*b*). In *International Tables for X-ray Crystallography*, Vol. II, p. 266, third equation (18). Birmingham: Kynoch Press. (Present distributor Kluwer Academic Publishers, Dordrecht.)

MILCH, J. R. & MINOR, T. C. (1974). The indexing of single-crystal X-ray rotation photographs. *J. Appl. Cryst.* **7**, 502–505.

MOORE, E. H. (1920). On the reciprocal of the general algebraic matrix. Abstract. *Bull. Am. Math. Soc.* **26**, 394–395.

MOORE, E. H. (1935). *General Analysis*. Philadelphia: American Philosophical Society.

PENROSE, R. (1955). A generalized inverse for matrices. *Proc. Cambridge Philos. Soc.* **51**, 406–413.

PETERS, G. & WILKINSON, J. H. (1970). The least squares problem and pseudo-inverses. *Comput. J.* **13**, 309–316.

RAO, C. R. & MITRA, S. K. (1971). *Generalized Inverse of Matrices and its Applications*, Preface, pp. vii–ix. New York: Wiley.

RENETSEDER, R., DIJKSTRA, B. W., KALK, K. H., VERPOORTE, J. & DRENTH, J. (1986). Bovine phospholipase A_2 crystals soaked in 30% methanol: the first structure determination with a FAST diffractometer at high resolution. *Acta Cryst.* B**42**, 602–605.

ROTH, M. & LEWIT-BENTLEY, A. (1986). Integration of single crystal neutron data using a PSD: a case of large, weak and often overlapping reflections. *J. Phys. (Paris) Colloq.* C5, Suppl. 8, **47**, 27–34.

SCHWARZENBACH, D. & FLACK, H.D. (1989). On the definition and practical use of crystal-based azimuthal angles. *J. Appl. Cryst.* **22**, 601–605.

STANSFIELD, R. F. D. (1983). Unpublished laboratory notes.

THOMAS, D. J. (1981). A useful algorithm in lattice geometry. *Acta Cryst.* A**37**, 553–557.

THOMAS, D. J. (1982*a*). Fast diffractometry. PhD thesis, Cambridge Univ., England.

THOMAS, D. J. (1982*b*). High-speed single-crystal television diffractometer (software). *Nucl. Instrum. Methods*, **201**, 27–30.

THOMAS, D. J. (1985). Computing for the Enraf–Nonius FAST system. In *Crystallographic Computing* 3: *Data Collection, Structure Determination, Proteins, and Databases*, edited by G. M. SHELDRICK, C. KRÜGER & R. GODDARD, pp. 52–60. Oxford: Clarendon Press.

THOMAS, D. J. (1986*a*). The development of a full profile analysis of single-crystal X-ray diffraction data. *J. Phys. (Paris) Colloq.* C5, Suppl. 8, **47**, 69–73.

THOMAS, D. J. (1986*b*). A general representation of polarisation. In Proc. of the EEC Cooperative Workshop on Position-Sensitive Detector Software (Phases I & II), LURE, 26 May – 7 June 1986, pp. 78–80.

THOMAS, D. J. (1986*c*). Suggestion of a unified description for all plane detectors. In Proc. of the EEC Cooperative Workshop on Position-Sensitive Detector Software (Phases I & II), LURE, 26 May – 7 June 1986, pp. 104–108.

THOMAS, D. J. (1986*d*). The impact of full profile analysis on program structure. In Proc. of the EEC Cooperative Workshop on Position-Sensitive Detector Software (Phases I & II), LURE, 26 May – 7 June 1986, pp. 112–120.

THOMAS, D. J. (1987). The balance between the relative capabilities of X-ray area detectors, computer and interface hardware, and software packages. In *Computational Aspects of Protein Crystal Data Analysis*, edited by J. R. HELLIWELL, P. A. MACHIN & M. Z. PAPIZ, pp. 162–170. Proc. of the Daresbury Study Weekend, 23–24 January 1987. Report DL/SCI/R25. SERC Daresbury Laboratory, Warrington, England.

THOMAS, D. J. (1989). Calibrating an area-detector diffractometer: imaging geometry. *Proc. R. Soc. London Ser. A*, **425**, 129–167.

THOMAS, D. J. (1990*a*). Modern equations of diffractometry. Goniometry. *Acta Cryst.* A**46**, 321–343.

THOMAS, D. J. (1990*b*). Calibrating an area-detector diffractometer: integral response. *Proc. R. Soc. London Ser. A*, **428**, 181–214.
THOMAS, D. J. (1992*a*). Manuscript on further diffraction geometry. In preparation.
THOMAS, D.J. (1992*b*). Manuscript on profile analysis. In preparation.
WESTFALL, R. S. (1980). *Never at Rest: a Biography of Isaac Newton*, p. 12. Cambridge Univ. Press.
WONACOTT, A. J. (1977). Geometry of the rotation method. In *The Rotation Method in Crystallography*, edited by U. W. ARNDT & A. J. WONACOTT, ch. 7, pp. 75–103. Amsterdam: North-Holland.

Acta Cryst. (1992). A**48**, 158–172

An Analytical Treatment of Disorder and Resolution of Atomic Electron-Density Functions for Carbon

BY THOMAS LAUBE

Laboratorium für Organische Chemie der Eidgenössischen Technischen Hochschule Zürich, ETH-Zentrum, Universitätstrasse 16, *CH*-8092 *Zürich, Switzerland*

(*Received* 26 *April* 1991; *accepted* 8 *August* 1991)

Abstract

Unresolved disorder can lead to structural distortions because of averaged atomic positions. The influence of the isotropic probability density function (p.d.f.), the distance between the disordered positions and the site occupation factors of a disordered C atom on the apparent position and anisotropic p.d.f. of the adjusted atom is studied with a simple model for the centrosymmetrical case. The electron density is derived from the STO-3G wave functions and convoluted analytically with the corresponding p.d.f. The optimal positional and displacement parameters are obtained by minimization of the integral of the square of the difference electron density. Several electron- and difference-density plots are shown in order to demonstrate the goodness of the adjustment and several correlations between the parameters of the disordered and adjusted atoms are discussed. The results are applied to some examples where unresolved disorder may be possible.

1. Introduction

Disorder occurs in the crystalline phases of many kinds of organic and inorganic compounds and may be the result of dynamic processes in a molecule or a crystal (dynamic disorder) or of two or more different orientations of a molecule in a crystal with similar energies (static disorder). If the different positions of an atom are resolved in an electron-density or difference-density map, it is in many cases possible to refine these positions with partial populations [assuming isotropic or anisotropic harmonic potentials (see *e.g.* Altona & Sundaralingam, 1972; Siegel, Gutiérrez, Schweizer, Ermer & Mislow, 1986)] or to describe this atom with an anharmonic potential (see *e.g.* Kuhs, 1983; Bachmann & Schulz, 1984). But if the disordered positions cannot be resolved due to a too small data set or due to the small distance between the positions, then the only hint of the presence of disorder is an unexpected shape or orientation of the displacement ellipsoid (Dunitz, Maverick & Trueblood, 1988; Dunitz, Schomaker & Trueblood, 1988). Some of the most persistent problems of physical organic chemistry are related to unresolved disorder because the different molecules or orientations of molecules are so similar that the distances between the disordered atomic positions are in the range of a few tenths of an ångström or even smaller. Well known examples are the structure of benzene (Ermer, 1987; Janoschek, 1987), antiaromatic systems (Dunitz, Krüger, Irngartinger, Maverick, Wang & Nixdorf, 1988), methanoannulenes (Bianchi, Pilati & Simonetta, 1981; Gatti, Barzaghi & Simonetta, 1985) and semibullvalenes (Jackman, Benesi, Mayer, Quast, Peters, Peters & von Schnering, 1989). Some inorganic examples were discussed by Chandrasekhar & Bürgi (1984). A similar problem occurs in the interpretation of the X-ray structures of substituted 8,9,10-trinorborn-2-yl and 8,9,10-trinorborn-2-en-7-yl cations (Laube, 1987, 1989), which could in principle also be described as superpositions of classical ions, if the anisotropic displacement parameters (ADPs) are ignored [for the problem of bridged and equilibrating carbocations, see *e.g.* Brown (1977); Olah, Prakash & Sommer (1985)]. In order to estimate the *maximal possible* distance between disordered positions hidden in ADPs, we analyse in this work with a simple model the influence of the distance between two disordered positions of a C atom, their site occupation factors and their isotropic displacement parameters on the *apparent* position and ADPs of this atom.

0108-7673/92/020158-15$03.00